

Inviscid damping of asymmetries on a two-dimensional vortex

D. A. Schecter, D. H. E. Dubin, A. C. Cass, C. F. Driscoll, I. M. Lansky, and T. M. O'Neil
Physics Department, University of California at San Diego, La Jolla, California 92093

(Received 7 January 1999; accepted 19 June 2000)

The inviscid damping of an asymmetric perturbation on a two-dimensional circular vortex is examined theoretically, and with an electron plasma experiment. In the experiment, an elliptical perturbation is created by an external impulse. After the impulse, the *ellipticity* (quadrupole moment) of the vortex exhibits an early stage of exponential decay. The measured decay rate is in good agreement with theory, in which the perturbation is governed by the linearized Euler equations. Often, the exponential decay of ellipticity is slow compared to a vortex rotation period, due to the excitation of a quasimode. A quasimode is a vorticity perturbation that behaves like a single azimuthally propagating wave, which is weakly damped by a resonant interaction with corotating fluid. Analytically, the quasimode appears as a wave packet of undamped continuum modes, with a sharply peaked frequency spectrum, and it decays through interference as the modes disperse. When the exponential decay rate of ellipticity is comparable to the vortex rotation frequency, the vorticity perturbation does not resemble a quasimode; rather, it is rapidly dominated by spiral filaments. Over longer times, linear theory predicts algebraic decay of ellipticity; however, nonlinear oscillations of ellipticity emerge in the experiment before a transition to algebraic decay would occur. © 2000 American Institute of Physics. [S1070-6631(00)01110-7]

I. INTRODUCTION

Many flows that occur in oceans, atmospheres, and plasmas are approximately two dimensional (2-D).¹⁻⁶ These flows are often dominated by a single vortex or by a group of interacting vortices. Although the vortex dynamics can be complicated, it is possible to gain a precise understanding of certain elementary processes. One example is the decay of an asymmetric perturbation on a stable circular vortex.⁷⁻²⁷

The decay of asymmetric perturbations on circular vortices can be studied experimentally with magnetized electron plasmas in a cylindrical Penning trap.⁷⁻⁹ We will show in Sec. IV that these electron plasmas evolve like inviscid incompressible 2-D fluids.

Figure 1 shows a typical experiment. At $t=0$, a circular vortex is deformed into an ellipse by an "external impulse" (described in Sec. III). After the impulse, the vortex relaxes toward an axisymmetric state, in a manner that resembles previous numerical simulations of 2-D Euler flow.¹⁰⁻¹³ During the relaxation, filaments form at a critical radius r_c , and vorticity contours become circular in the core of the vortex. Moreover, the ellipticity of the vortex decays *exponentially* by one order of magnitude, before oscillating and reaching a terminal value. Here, the ellipticity is measured by the amplitude of the quadrupole moment of the perturbed vortex [the $m=2$ multipole moment, defined by Eq. (12)].

We will show (in Sec. IV) that the initial stage of exponential decay in the experiments is governed by the linearized Euler equations. Over longer times, linear theory predicts that the quadrupole moment will decay algebraically (like $t^{-\alpha}$).^{17,28,29} However, in the experiments, nonlinear effects emerge before a transition to algebraic decay would occur. These nonlinear effects include the "trapping oscillations" and equilibration of ellipticity in Fig. 1(b).

Before analyzing the experiments in greater detail, we will elaborate upon the linear theory of perturbations that are created by an external impulse. We will show that in linear theory, an external impulse often excites a "quasimode." A quasimode is a vorticity perturbation that behaves (early on) like a single exponentially damped wave in the vortex core, with frequency ω_q and decay rate γ . The decay rate of the quasimode is slow compared to its oscillation frequency; that is, $\gamma/\omega_q \ll 1$. Moreover, the decay rate is proportional to the vorticity gradient at the critical radius r_c , where the vortex rotation frequency $\Omega_0(r)$ satisfies the resonance condition, $m\Omega_0(r_c) = \omega_q$ ($m=2$ for an elliptical perturbation). This indicates that the early exponential decay of the quasimode is due to a resonant wave-fluid interaction,^{14,30} as explained in Appendix A.

By its name, one can infer that a quasimode is not a genuine eigenmode of the vortex: the monotonic vortices that we treat here do not support exponentially damped eigenmodes.¹⁴ After a general discussion of eigenmode theory (in Sec. II), we will show that the quasimode appears analytically as a wave packet of undamped "continuum modes," with a sharply peaked frequency spectrum.³¹ The peak of the spectrum is well described by a Lorentzian of width γ , centered at ω_q . The wave packet decays through interference as the continuum modes disperse. When the vorticity gradient at r_c is zero, γ is also zero, and the wave packet (quasimode) is replaced by a single undamped "discrete mode."

The quasimodes of a circular vortex have been studied previously in the context of a Laplace transform solution to the initial value problem.¹⁴⁻¹⁶ In this approach, the frequency ω_q and decay rate γ of a quasimode appear as the real and imaginary parts of a "Landau pole." A Landau pole is a

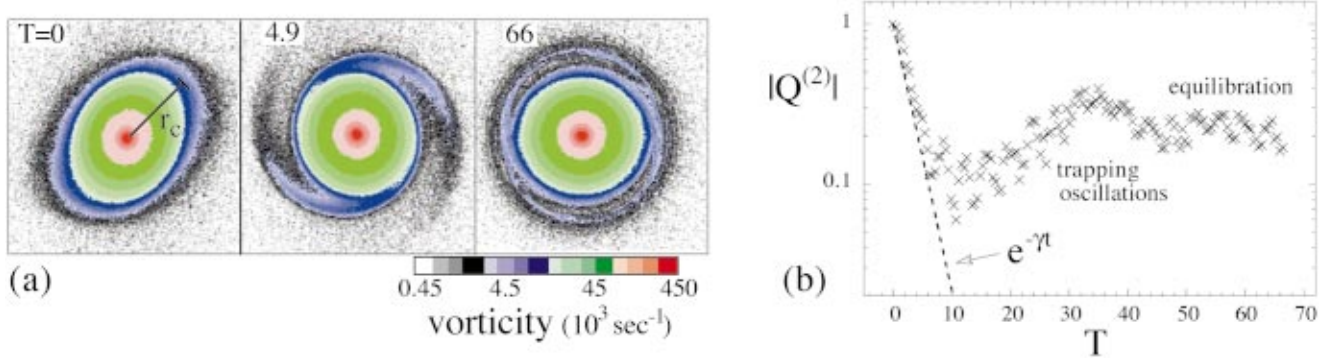


FIG. 1. (Color) Electron plasma experiment. (a) The evolution of vorticity after an elliptical perturbation is applied to an initially circular vortex. As filamentation occurs at r_c , the vorticity contours relax back to circular form in the vortex core ($r \leq r_c$). (b) The relaxation of the quadrupole moment (ellipticity). The dashed line indicates that the initial decay is exponential. Time is measured in central rotation periods, $T = t\Omega_0(0)/2\pi$. The amplitude $|Q^{(2)}(t)|$ of the quadrupole moment is in units of $|Q^{(2)}(0)|$.

complex frequency at which the temporal Laplace transform of the quadrupole moment is singular: its value depends only on the equilibrium vorticity profile, and not the initial perturbation (see Appendix B). Of course, the values of ω_q and γ obtained from the Landau pole agree with those obtained from our eigenmode analysis of the quasimode.

We will also consider a case where the vortex (a Gaussian) has a Landau pole with a large imaginary part ($\gamma/\omega_q \sim 1$). In this case, we show that the vorticity perturbation evolving from an external impulse does not resemble a single damped wave (quasimode). Rather, the vorticity perturbation becomes dominated by spiral filaments in a few vortex rotation periods.^{17–21} Surprisingly, the quadrupole moment (ellipticity) of this perturbation decays exponentially, at a rate given by the Landau pole. So, “Landau damping” is physically relevant even if the vortex appears to have no quasimode.

After reviewing and elaborating upon linear response theory, we will examine the initial behavior of the experimental vortices more thoroughly. We will show that the observed exponential decay of the quadrupole moment is accurately given by a Landau pole of the vortex. We will also show that the spatial structure of an experimental quasimode, as well as its frequency and decay rate are in good quantitative agreement with linear theory.

We now give an outline of the main text. In Sec. II, we review the eigenmode approach to the study of linear perturbations on a circular vortex.^{26,27} We then examine the quasimodes of circular vortices, in the context of eigenmode theory. In Sec. III, we present the linear theory of (elliptical) perturbations that are created by an external impulse. In Sec. IV, we show that the experiments agree quantitatively with linear response theory. In Appendix A, we provide a physical picture of the resonant wave–fluid interaction^{14,30} that causes exponential decay. In Appendix B, we review how to calculate Landau poles numerically.¹⁶

II. EIGENMODE THEORY

In this section, we review and extend upon the eigenmode theory of small perturbations on a 2-D vortex.^{26,27,32} This provides necessary background for Secs. III and IV.

A. The eigenmode expansion

We assume that the vortex is governed by the 2-D Euler equations, which neglect compressibility and viscosity:

$$\frac{\partial \zeta}{\partial t} + \mathbf{v} \cdot \nabla \zeta = 0, \quad \mathbf{v} = \hat{z} \times \nabla \psi, \quad \nabla^2 \psi = \zeta. \quad (1)$$

Here, $\mathbf{v}(r, \theta, t)$ is the velocity field, $\zeta(r, \theta, t) \equiv \hat{z} \cdot \nabla \times \mathbf{v}$ is the vorticity, and $\psi(r, \theta, t)$ is a stream function. We also assume that the fluid is bounded by a circular wall at which there is free slip, i.e., $\psi = 0$ at the wall radius R_w .

The vorticity distribution in the flow can be decomposed into an axisymmetric equilibrium $\zeta_0(r)$ and a perturbation $\Delta \zeta(r, \theta, t)$; that is,

$$\zeta(r, \theta, t) \equiv \zeta_0(r) + \Delta \zeta(r, \theta, t). \quad (2)$$

Furthermore, the perturbation can be expressed as a Fourier series in the polar angle θ ,

$$\Delta \zeta(r, \theta, t) \equiv \delta \zeta^{(0)}(r, t) + \sum_{m=1}^{\infty} \{ \delta \zeta^{(m)}(r, t) e^{im\theta} + \text{c.c.} \}. \quad (3)$$

If the perturbation is sufficiently small, it is approximately governed by the linearized Euler equations. These equations are obtained by neglecting second-order perturbation terms in Eq. (1), and can be written for each Fourier component separately:

$$\frac{\partial \delta \zeta}{\partial t} + im \Omega_0(r) \delta \zeta - \frac{im}{r} \zeta_0'(r) \delta \psi = 0, \quad (4a)$$

$$\left[\frac{1}{r} \frac{\partial}{\partial r} r \frac{\partial}{\partial r} - \frac{m^2}{r^2} \right] \delta \psi = \delta \zeta. \quad (4b)$$

Here, $\Omega_0(r)$ is the unperturbed angular rotation frequency of the vortex, and $\zeta_0'(r)$ is the radial derivative of the equilibrium vorticity distribution. In addition, $\delta \psi(r, t)$ is the (m th) Fourier coefficient of the stream function perturbation. The superscript “(m)” has been dropped to simplify notation.

Equation (4b) can be solved formally with a Green’s function technique, yielding

$$\delta\psi(r,t) = \int_0^{R_v} dr' r' G(r|r') \delta\zeta(r',t), \quad (5)$$

where R_v is the radius of the vortex. For the asymmetric components of the perturbation ($m \geq 1$), the Green's function $G(r|r')$ is given by

$$G(r|r') = -\frac{1}{2m} \left(\frac{r_{<}}{r_{>}} \right)^m \left[1 - \left(\frac{r_{>}}{R_w} \right)^{2m} \right], \quad (6)$$

where $r_{>}$ ($r_{<}$) is the larger (smaller) of r and r' . This Green's function incorporates the boundary condition $\delta\psi = 0$ at $r = R_w$.

The linearized Euler equations support azimuthally propagating waves, i.e., Eqs. (4a) and (4b) have solutions of the form $\delta\zeta = \xi(r)e^{-i\omega t}$. These waves are either "discrete modes" or "continuum modes." Each Fourier component of the vorticity perturbation can be expressed as a sum of discrete modes, plus an integral of continuum modes,^{26,27,31,33,34} that is,

$$\delta\zeta(r,t) = \sum_d A(\omega_d) \xi_d(r) e^{-i\omega_d t} + \int d\omega A(\omega) \xi_\omega(r) e^{-i\omega t}. \quad (7)$$

The discrete modes have radial eigenfunctions $\xi_d(r)$ that are spatially smooth. Therefore, a discrete mode is a physical solution to the linearized Euler equations. On the other hand, the eigenfunction of a continuum mode has a singular point at the radius where the fluid co-rotates with that mode (see Sec. II C).^{27,33,34} Consequently, only an integral of continuum modes has physical meaning.

The eigenvalue equation for these modes can be written as²⁶

$$I[\xi(r)] = \omega \xi(r), \quad (8)$$

where I is the linear integral operator defined below:

$$I[\xi] \equiv m\Omega_0(r)\xi(r) - \frac{m}{r} \zeta'_0(r) \int_0^{R_v} dr' r' G(r|r') \xi(r'). \quad (9)$$

Equation (8) is obtained by substituting an eigenmode solution $\delta\zeta = \xi(r)e^{-i\omega t}$ into Eq. (4a), and using Eq. (5) for $\delta\psi$.

In practice, the integral eigenvalue equation [Eq. (8)] is solved numerically. The radial coordinate r is discretized into N (typically 10^2 – 10^4) grid points between 0 and R_v , and the operator I is converted into an $N \times N$ matrix.³⁵ The resulting matrix eigenvalue equation is solved with a standard routine.³⁶

The solution gives N eigenfrequencies $\{\omega_k\}$ and N eigenfunctions (eigenvectors) $\{\xi_k(r)\}$. They are used to form an approximate (i.e., numerical) solution to the initial value problem:

$$\delta\zeta(r,t) = \sum_{k=1}^N A_k \xi_k(r) e^{-i\omega_k t}. \quad (10)$$

This sum over k includes the discrete modes, and a finite representation of the continuum modes.

Because the numerical solution [Eq. (10)] has only a finite number of continuum modes, it breaks down after a time $\tau \sim 2\pi/\Delta\omega_{\max}$. Here, $\Delta\omega_{\max}$ is the maximum frequency

spacing between two neighboring continuum modes. For all numerical results in this paper, $\Delta\omega_{\max}$ is made sufficiently small (by increasing N) to keep τ larger than the time scale of interest.

The expansion coefficients $\{A_k\}$ in Eq. (10) depend on how the eigenfunctions $\{\xi_k\}$ are normalized. With the exception of a single case, discussed in connection with Fig. 10, we let

$$\int_0^{R_v} dr r^{m+1} \xi_k(r) = b, \quad (11)$$

where b has the same value for all modes (the exact value of b is unimportant). In Sec. II D, we will show that Eq. (11) is a convenient normalization for analyzing quasimodes. Of course, Eq. (11) can not be used if the integral vanishes for any eigenfunction ξ_k .

By using Eq. (11) for the normalization, we also establish a direct proportionality between the eigenmode amplitudes and the frequency spectra of the perturbation's multipole moments. We define the m th multipole moment of a vorticity perturbation by

$$Q^{(m)}(t) \equiv \int_0^{R_v} dr r^{m+1} \delta\zeta^{(m)}(r,t). \quad (12)$$

The amplitude and phase of the m th multipole moment measure the strength and orientation of the wave-number m asymmetry. Each multipole moment can be written as a sum over eigenmode contributions; that is, $Q(t) = \sum_{k=1}^N q_k e^{-i\omega_k t}$. Substituting Eq. (10) into Eq. (12) gives $q_k = bA_k$, provided that $\int_0^{R_v} dr r^{m+1} \xi_k(r) = b$.

B. The eigenmodes of a general monotonic vortex

The experimental vortices are monotonic. That is, their equilibrium vorticity profiles decrease monotonically with radius r , until reaching zero at the vortex radius R_v :

$$\begin{aligned} \zeta'_0(r) &< 0 \quad \text{for } 0 < r < R_v, \\ \zeta_0(r) &= 0 \quad \text{for } r \geq R_v. \end{aligned} \quad (13)$$

In this section, we briefly state the general properties of the eigenmodes of a monotonic vortex.

All eigenfrequencies of a monotonic vortex are real, so all eigenmodes are neutrally stable.³⁷ This is because the integral operator I , appearing in the eigenmode equation [Eq. (8)], is Hermitian with respect to the inner-product

$$\langle f, h \rangle \equiv \int_0^{R_v} dr \frac{r^2}{|\zeta'_0(r)|} f^*(r) h(r). \quad (14)$$

That is,

$$\langle f, I[h] \rangle = \langle h, I[f] \rangle^*. \quad (15)$$

The Hermiticity of I also guarantees that its eigenfunctions form a complete orthogonal set.

Orthogonality can be used to derive the following expression for the coefficients $\{A_k\}$ in the eigenmode expansion [Eq. (10)]:

$$A_k = \frac{\langle \xi_k, \delta\zeta(r,0) \rangle}{\langle \xi_k, \xi_k \rangle}. \quad (16)$$

Here, $\delta\zeta(r,0)$ is the Fourier coefficient of the vorticity perturbation at time $t=0$. To evaluate the inner-products in Eq. (16), we use trapezoidal integration.³⁵

We note that the inner-product in Eq. (14) is defined only if $\zeta'_0 \neq 0$ for all $r < R_v$. Therefore, the results derived here do not necessarily apply to nonmonotonic vortices. For example, a nonmonotonic vortex can have complex eigenfrequencies, corresponding to unstable modes.

C. The eigenmodes of a top-hat vortex with a discrete mode

The eigenmodes of a monotonic vortex are best described through an example. Here, we consider a vortex where $\zeta_0(r)$ slowly decreases from $r=0$ to $r=r_0$, and then rapidly drops to zero in a transition layer of width δr . This vortex is shown in Fig. 2 (top), and will be referred to as *Top-Hat 1*. Although the exact functional form of Top-Hat 1 is not important, it is provided in the following:

$$\zeta_0(r) = \begin{cases} 0.485 \left[1 - 1.01 \tanh\left(\frac{r-r_0}{\delta r}\right) \right] \left[1 + 0.025 \left(\frac{R_v-r}{R_v}\right) \right], & r < R_v \\ 0, & r \geq R_v, \end{cases} \quad (17)$$

where $\delta r = 0.01$, $r_0 = 0.3$, and the vortex radius is $R_v = 0.327$. Here, *and throughout this paper*, all lengths are given in units of the wall radius R_w . In addition, all frequencies are given in units of $\zeta_0(0)$. Thus, $\zeta_0(0) = 1$ in Eq. (17).

The $m=2$ eigenmodes of Top-Hat 1 typify the eigenmodes for all m . As is generally the case, the $m=2$ numerical eigenspectrum has a set of eigenfrequencies that fall in the range

$$m\Omega_0(R_v) < \omega_k < m\Omega_0(0). \quad (18)$$

As the number of radial grid-points N increases, this subset of $(N-1)$ eigenfrequencies becomes increasingly dense between the upper and lower limits; therefore, it represents the continuum.

Figure 2 (bottom) shows the radial eigenfunction of a generic continuum mode. The radial eigenfunction ξ_k of each continuum mode has a singular spike at its critical radius $r_{c,k}$, defined by

$$m\Omega_0(r_{c,k}) \equiv \omega_k. \quad (19)$$

Physically, the critical radius is where the unperturbed fluid corotates with the eigenmode. The critical radii of the continuum modes span the interval from $r=0$ to $r=R_v$.

The $m=2$ eigenspectrum of Top-Hat 1 also has a discrete eigenfrequency ω_d , which lies outside the continuum [$\omega_d = 0.496 < m\Omega_0(R_v)$]. The critical radius r_c of this discrete mode is defined by the resonance condition, $m\Omega_0(r_c) \equiv \omega_d$. It has the value $r_c = 0.42 > R_v$. Because r_c is greater

than R_v , the eigenmode equation [Eq. (8)] is not singular, and the radial eigenfunction $\xi_d(r)$ of the discrete mode does not have a singular spike.

It is possible to derive an approximate analytic expression for the radial eigenfunction of the discrete mode. The result is

$$\xi_d(r) \approx \alpha \frac{G(r|r_0)}{m\Omega_0(r) - \omega_d} \frac{1}{r} \zeta'_0(r), \quad (20)$$

where α is a constant that is determined by the normalization [e.g., Eq. (11)]. Equation (20) is obtained from the integral eigenvalue equation [Eq. (8)] under the assumption that $\zeta'_0(r)$ is sharply peaked at r_0 . In Fig. 2, Eq. (20) is compared to the $m=2$ discrete eigenfunction of Top-Hat 1. The two are in excellent agreement.

Because Top-Hat 1 resembles a uniform circular vortex patch (of radius $r_0 = R_v$), its discrete modes resemble those of a uniform circular vortex patch. A dispersion relation for these modes was derived in 1880 by Kelvin.³² The frequency of the discrete mode with azimuthal wave-number m is given by

$$\omega_d = \frac{1}{2} \left[m-1 + \left(\frac{r_0}{R_w}\right)^{2m} \right], \quad (21)$$

and its critical radius is

$$r_c = r_0 \left[\frac{m}{m-1 + (r_0/R_w)^{2m}} \right]^{1/2}. \quad (22)$$

In Eq. (21), ω_d is in units of ζ_0 , the constant vorticity of the patch. With $m=2$ and $r_0=0.3$ (in units of R_w), Eq. (21) gives $\omega_d = 0.504$, and Eq. (22) gives $r_c = 0.42$. These results are in good agreement with the numerical values of ω_d and r_c for Top-Hat 1 that were stated previously.

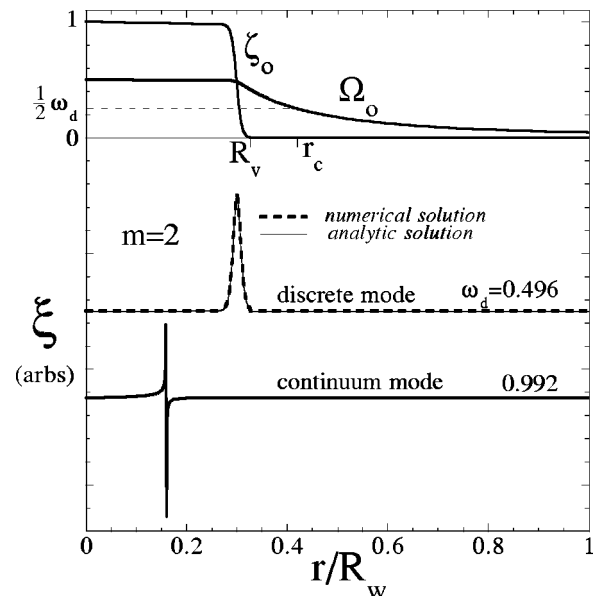


FIG. 2. Top-Hat 1. Equilibrium profile and two radial eigenfunctions from the $m=2$ spectrum. The eigenfunctions are zero at $r=0$, but are offset for clarity. Both are scaled arbitrarily. The markings ω_d and r_c denote the frequency and critical radius (respectively) of the discrete mode.

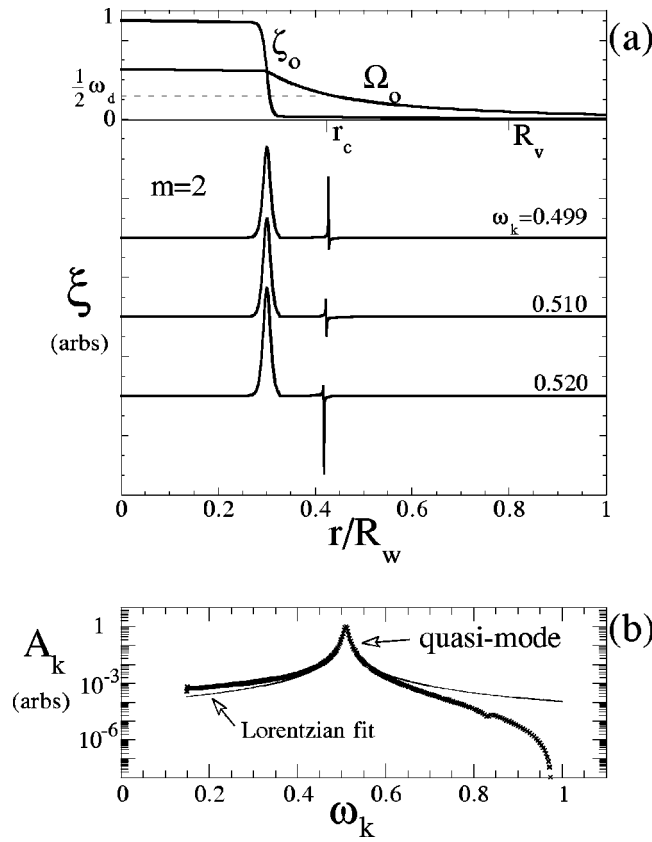


FIG. 3. Top-Hat 2. (a) Equilibrium profile and radial eigenfunctions of the $m=2$ “exceptional” continuum modes. The eigenfunctions are zero at $r=0$, but are offset for clarity. They are also shown on the same scale. The markings ω_d and r_c denote the frequency and critical radius (respectively) of the $m=2$ discrete mode of Top-Hat 1. (b) Expansion coefficients $\{A_k\}$ for the discrete eigenfunction $\xi_d(r)$ of Top-Hat 1, expanded in the continuum eigenfunctions of Top-Hat 2.

Although we have focused on a monotonic vortex with a single sharp edge at r_0 , it is important to note that discrete modes exist on monotonic vortices of many kinds. For example, discrete modes can exist even when the vorticity gradient ζ'_0 is roughly constant across the entire vortex. If there are multiple peaks in ζ'_0 , then there can be multiple peaks in the radial eigenfunction of the discrete mode. In short, discrete modes can be found in a wide variety of forms.

D. Discrete mode to quasimode

Top-Hat 2 in Fig. 3(a) is equivalent to Top-Hat 1, with the addition of a low-vorticity skirt that extends radially to $R_v=0.8$. This skirt broadens the continuous spectrum of eigenfrequencies [Eq. (18)], bringing its lower limit $m\Omega_0(R_v)$ below the eigenfrequency ω_d of the original discrete mode. Consequently, all eigenmodes of Top-Hat 2 are continuum modes.

However, the discrete mode of Top-Hat 1 has not disappeared entirely. The continuum modes of Top-Hat 2 that are shown in Fig. 3(a) closely resemble the original discrete mode. To begin with, they have eigenfrequencies near ω_d . Also, their radial eigenfunctions are approximately $\xi_d(r)$, except for minor spikes near r_c . We will refer to these and other continuum modes with frequencies near ω_d as “excep-

tional,” because they have exceptionally large inner-products with the original discrete mode.

The exceptional continuum modes have an important physical significance: they combine to form a quasimode. Consider the discrete mode of Top-Hat 1 as an initial condition on Top-Hat 2; that is, $\delta\zeta(r,0)=\xi_d(r)$. This initial condition will now evolve as a superposition of continuum modes. Figure 3(b) shows the expansion coefficients A_k vs ω_k . The distribution is sharply peaked near the eigenfrequency ω_d . A Lorentzian distribution accurately describes the peak,

$$A_k \sim \frac{1}{(\omega_k - \omega_q)^2 + \gamma^2}, \quad (23)$$

with $\omega_q=0.509$ and $\gamma=5 \times 10^{-3}$. In Sec. III [Eq. (31)], we will show that the value of γ is proportional to the vorticity gradient at the critical radius; for Top-Hat 2, $\zeta'_0(r_c)=6.07 \times 10^{-2} \zeta_0(0)/R_w$.

As the continuum modes disperse, their superposition behaves like an exponentially damped version of the original discrete mode. To see this, we first approximate the eigenmode expansion [Eq. (10)] by

$$\delta\zeta(r,t) \approx \xi_d(r) \sum_k A_k e^{-i\omega_k t}, \quad (24)$$

for $r \leq r_c = 0.42$. This simplification is possible since (i) the peak region of A_k dominates the expansion, and (ii) the exceptional continuum modes have eigenfunctions $\{\xi_k\}$ that roughly equal the eigenfunction ξ_d of the original discrete mode, for $r \leq r_c$. Substituting the Lorentzian form of A_k [Eq. (23)] into Eq. (24), we obtain the desired result: $\delta\zeta \approx \xi_d(r) e^{-(\gamma+i\omega_q)t}$ for $r \leq r_c$.

Note that our analysis of the quasimode was simplified by the way that we chose to normalize the eigenfunctions [Eq. (11)]. With this normalization, the eigenmodes in the peak region of A_k have eigenfunctions [Fig. 3(a)] that are approximately equivalent: $\xi_k(r) \approx \xi_d(r)$ for $r \leq r_c$. With a different normalization, these eigenfunctions would vary in size. As a result, A_k would not have a Lorentzian form, and a Lorentzian fit would give inaccurate values for the frequency ω_q and decay rate γ of the quasimode.

As a final remark, quasimodes (like discrete modes) exist on vortices of many kinds. Here, we have focused on a top-hat vortex, in which case the radial “eigenfunction” of the quasimode has a single sharp peak. However, on different vortices, quasimodes can have broad “eigenfunctions” with multiple peaks: the variety of quasimodes is infinite, just as the variety of discrete modes is infinite.

III. LINEAR RESPONSE OF A MONOTONIC VORTEX TO AN EXTERNAL IMPULSE

A. Eigenmode excitability

In the experiments, an “external impulse” is applied to the vortex, creating an elliptical perturbation. In linear theory, this perturbation will evolve as a superposition of freely propagating eigenmodes [Eq. (10)]. In the following,

we derive an equation for the distribution of eigenmode amplitudes in the impulse-generated perturbation.

The external impulse is a weak flow field that is briefly superimposed on the vortex. The stream function of this flow field is given approximately by

$$\psi_{\text{ext}}(r, \theta, t) = f(t) \left(\frac{r}{R_w} \right)^m e^{im\theta} + \text{c.c.}, \quad (25)$$

with $m=2$. The time-dependent factor $f(t)$ is assumed to be nonzero for only a brief interval. The radial factor varies like r^m inside the vortex, because the source of the impulse is at the wall (external to the vortex), i.e., $\nabla^2 \psi_{\text{ext}} = 0$ for $r < R_w$. In Sec. IV, we will explain how the external impulse is applied in practice.

We treat the external impulse as a perturbation, and assume that the Euler equation for the evolution of vorticity can be linearized during and after the impulse. Including the stream function of the external impulse, the linearized vorticity equation is

$$\frac{\partial \delta \zeta}{\partial t} + iI[\delta \zeta] = \frac{im}{(R_w)^m} f(t) r^{m-1} \zeta'_0. \quad (26)$$

Here, I is the linear integral operator that is defined by Eq. (9). Equation (26) was obtained by making the substitution $\delta \psi \rightarrow \delta \psi + \delta \psi_{\text{ext}}$ in Eq. (4a).

The Fourier coefficient of the vorticity perturbation can be expanded in the (discretized) eigenfunctions of I ; that is, $\delta \zeta(r, t) = \sum_{k=1}^N a_k(t) \xi_k(r)$. Furthermore, Eq. (26) can be rewritten as a set of N independent equations, one for each $a_k(t)$. These first-order ordinary differential equations can be solved by standard methods.³⁵ It is found that after the impulse, $a_k(t) = A_k e^{-i\omega_k t}$, with

$$A_k = - \frac{im}{(R_w)^m} X_k F_k^*. \quad (27)$$

Here, F_k^* is the complex conjugate of the Fourier transform of $f(t)$, evaluated at ω_k . The quantity X_k is the ‘‘eigenmode excitability,’’ defined by

$$X_k \equiv - \frac{\langle \xi_k, r^{m-1} \zeta'_0 \rangle}{\langle \xi_k, \xi_k \rangle} = \frac{\int_0^{R_w} r^{m+1} \xi_k(r) dr}{\langle \xi_k, \xi_k \rangle}. \quad (28)$$

The first equality states that X_k is (minus) the expansion coefficient of the function $r^{m-1} \zeta'_0$. The second equality makes use of Eq. (14), which defines the inner-product: It states that the excitability X_k is the multipole moment of the k th eigenmode, divided by the weight $\langle \xi_k, \xi_k \rangle$ of that eigenmode.

In the experiments, the external impulse is typically applied over a time interval much less than the turnover time of the vortex ($\sim 2\pi/\Omega_0$). It is therefore reasonable to approximate $f(t)$ with a delta function of strength ϵ ; that is, $f(t) = \epsilon \delta(t)$. Then, $F_k^* = \epsilon$ for all ω_k , and Eq. (27) yields

$$A_k = - \frac{im \epsilon}{(R_w)^m} X_k. \quad (29)$$

So, the amplitude of the k th eigenmode after a $\delta(t)$ external impulse is directly proportional to X_k . The vorticity perturbation immediately after the impulse is given by

$$\delta \zeta(r, 0) = \frac{im \epsilon}{(R_w)^m} r^{m-1} \zeta'_0(r). \quad (30)$$

This result is obtained from the expansion $\delta \zeta(r, 0) = \sum_{k=1}^N A_k \xi_k(r)$, using Eq. (29) for A_k , and then Eq. (28) for X_k .

Finally, Eq. (29) implies that the eigenmodes satisfy a reciprocity principle. Substituting Eq. (28) for X_k into Eq. (29), one finds that eigenmodes of the same weight $\langle \xi_k, \xi_k \rangle$ are excited in proportion to their multipole moments. In this sense, the eigenmodes with the strongest influence on the external flow are also the most sensitive to a brief disturbance that is created by an external source.

B. The excitation of a quasimode on a top-hat vortex

We now show that an external impulse excites a quasimode on a top-hat vortex, and that this quasimode decays at a rate given by a Landau pole.

Suppose that Top-Hat 2 (Fig. 3) is perturbed by an $m=2$, $\delta(t)$ external impulse. This impulse creates a vorticity perturbation of the form $\delta \zeta(r, t) e^{i2\theta} + \text{c.c.}$ In Sec. III A, we showed that $\delta \zeta \propto \sum_{k=1}^N X_k \xi_k(r) e^{-i\omega_k t}$, for $t > 0$. Here, X_k is the eigenmode excitability that is defined by Eq. (28). Figure 4(a) shows X_k as a function of ω_k , for eigenmodes normalized by Eq. (11). This excitability spectrum is sharply peaked near the exceptional continuum modes of the vortex [e.g., the modes in Fig. 3(a)]. Moreover, the peak in X_k has the same Lorentzian structure (solid line) as the quasimode expansion that was described in Sec. II [Eq. (23)]; therefore, the impulse excites a quasimode.

Figures 4(b) and 5 illustrate that this quasimode behaves early on like a single exponentially damped wave. Figure 4(b) shows the vorticity perturbation at $T=0$ and at $T=30$ central rotation periods. During this time interval, the vorticity perturbation (for $r \lesssim 0.33$) decays an order of magnitude, and rotates with a phase velocity that is independent of both time and radius; that is, the vorticity perturbation behaves like a single damped wave. Figure 5 verifies that the amplitude $|Q^{(2)}(t)|$ of the quadrupole moment [Eq. (12)] decays exponentially after the impulse. As expected, the exponential decay rate is $\gamma = 5 \times 10^{-3}$ in units of $\zeta_0(0)$; previously, we obtained this value of γ by fitting the expansion coefficients of the quasimode to a Lorentzian function of ω_k [Eq. (23)].

The exponential decay rate can also be obtained from a Landau pole of the equilibrium profile.^{14–16} A ‘‘Landau pole’’ is a complex frequency, $\omega_q - i\gamma$, at which the Laplace transform of $Q^{(m)}(t)$ is singular: it depends only on the equilibrium profile, and not the specific perturbation (see Appendix B). A Landau pole contributes a term to $Q^{(m)}(t)$ of the form $e^{-\gamma t} e^{-i\omega_q t}$; however, this term cannot represent a complete solution to the initial value problem (unless $\gamma=0$).

The Landau pole for a top-hat vortex was calculated analytically by Briggs, Daugherty, and Levy.¹⁴ This Landau pole gives the following decay rate:

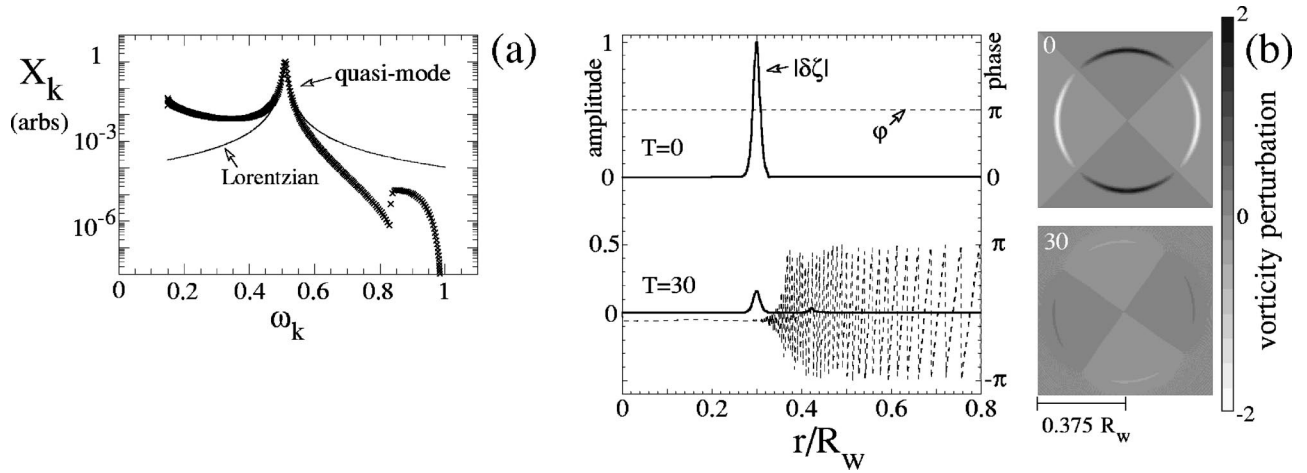


FIG. 4. The excitation and decay of an $m=2$ quasimode on Top-Hat 2. (a) The sharply peaked excitability spectrum indicates the excitation of a quasimode. (b) The vorticity perturbation, $\Delta\zeta(r, \theta, t) = 2|\delta\zeta(r, t)|\cos[m\theta + \varphi(r, t)]$. The left graph in (b) shows the half-amplitude $|\delta\zeta|$ and phase φ of the perturbation as functions of radius, at $T=0$ and at $T=30$ central rotation periods [$T = t\Omega_0(0)/2\pi$]. The right figures in (b) are contour plots of $\Delta\zeta$.

$$\gamma_{\text{BDL}} \approx \frac{-\pi}{4m} r_0 \zeta'_0(r_c) \left(\frac{r_0}{r_c}\right)^{2m-3} \left[1 - \left(\frac{r_c}{R_w}\right)^{2m}\right]^2. \quad (31)$$

Here, r_0 is the radius where $|\zeta'_0(r)|$ is maximal, and r_c is the critical radius of the quasimode, given approximately by Eq. (22). Figure 5 shows that γ_{BDL} gives the correct exponential decay rate of the quadrupole moment after an external impulse disturbs Top-Hat 2.

In Appendix A, we present an alternative derivation of the exponential decay rate that is given by Eq. (31). This derivation shows explicitly how the observed exponential damping occurs through an exchange of angular momentum between the quasimode and corotating fluid elements at r_c .

It is worth emphasizing that quasimodes are not genuine exponentially damped eigenmodes: such eigenmodes do not exist on a monotonic vortex. There are two features that distinguish the evolution of a quasimode from the evolution of a damped eigenmode. First, the quadrupole moment of the quasimode makes a transition toward algebraic decay; here, at approximately 100 rotation periods (see Fig. 5). Second, as the original vorticity perturbation decays, a smaller perturbation grows in a thin layer about the critical radius, $r_c = 0.42$. Eventually, the amplitude of this smaller perturbation saturates, but its phase continues to evolve.

The structure of the ‘‘bump’’ at r_c can be calculated analytically. During the growth of the bump, the stream function perturbation is dominated by the vorticity perturbation in the vortex core ($r \lesssim r_c$). In the core, $\delta\zeta \approx \beta r^{m-1} \zeta'_0(r) e^{-(\gamma_{\text{BDL}} + i\omega_d)t}$, where ω_d is given by Eq. (21), and γ_{BDL} is defined by Eq. (31). The coefficient β is determined by the initial condition [Eq. (30)] that is created by the impulse; accordingly, $\beta = im\epsilon/(R_w)^m$. Taking $\zeta'_0 \approx -\zeta_0(0)\delta(r-r_0)$, and using Eq. (5) for the stream function perturbation, we obtain

$$\delta\psi \approx -im\epsilon \left(\frac{r_0}{R_w}\right)^m \zeta_0(0) G(r|r_0) e^{-(\gamma_{\text{BDL}} + i\omega_d)t}. \quad (32)$$

Here, G is the Green’s function that is given by Eq. (6).

The evolution of $\delta\zeta$ in the region of the bump (near r_c) is obtained by integrating Eq. (4a), with $\delta\psi$ given by Eq. (32). In this region, one finds that

$$\lim_{t \rightarrow \infty} |\delta\zeta| \approx -\frac{1}{2} \frac{|\epsilon| \zeta'_0(r_c) (r_0/R_w)^m (r_0/r_c)^{m-2} [1 - (r_c/R_w)^{2m}]}{\sqrt{(\gamma_{\text{BDL}} r_c^3 / m \zeta_0(0) r_0^2)^2 + (r - r_c)^2}}. \quad (33)$$

In deriving Eq. (33), we used Eq. (6) for the Green’s function, and we assumed that $\Omega_0(r) \approx [\zeta_0(0)/2](r_0/r)^2$ for $r > r_0$. Figure 6 shows that there is good agreement between Eq. (33) and the vorticity bump that develops in the skirt of Top-Hat 2.

Equation (33) indicates that the radial width of the bump is proportional to the decay rate $\gamma \approx \gamma_{\text{BDL}}$ of the quasimode. This relationship is simple to understand if the quasimode is viewed as a wave packet of continuum modes. The decay rate γ is the peak width of the wave packet’s frequency spectrum, X_k . The peak width defines a critical layer in the vortex, where the continuum modes are resonant with the fluid rotation and have singular spikes: The radial thickness

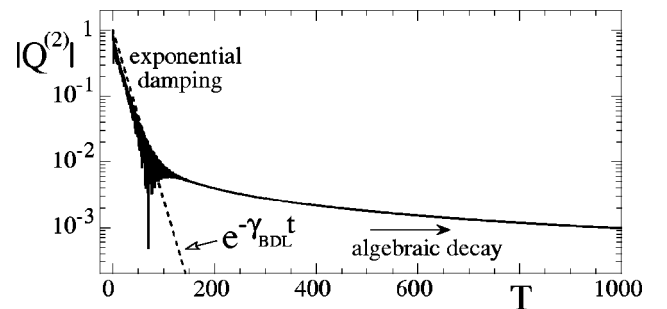


FIG. 5. Evolution of the quadrupole moment of Top-Hat 2 after an external impulse. The dashed line indicates exponential damping, with decay rate given by Eq. (31). $|Q^{(2)}(t)|$ is in units of $|Q^{(2)}(0)|$; $T = t\Omega_0(0)/2\pi$.

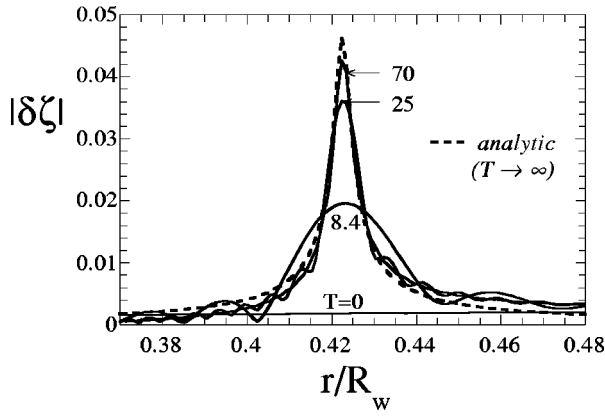


FIG. 6. Growth of $|\delta\zeta|$ in the critical layer. The dashed line is Eq. (33). The vorticity units are the same as in Fig. 4(b). $T = t\Omega_0(0)/2\pi$.

of this critical layer is approximately $\gamma/m\Omega'_0(r_c)$. As the continuum modes disperse, the singular spikes unravel, forming a bump across the critical layer.

We now briefly discuss the response of Top-Hat 1 (Fig. 2) to a $\delta(t)$ external impulse. Top-Hat 1 supports an undamped discrete mode, since it has zero vorticity gradient at r_c . Figure 7 shows the $m=2$ excitability spectrum $\{X_k\}$ of Top-Hat 1. It is apparent that the discrete mode dominates the impulse generated perturbation. This is because the eigenfunction ξ_d of the discrete mode, given by Eq. (20), roughly equals the initial perturbation [Eq. (30)]; that is, $\xi_d(r) \approx \delta\zeta(r,0) \propto r^{m-1}\zeta'_0(r)$. Since the continuum eigenfunctions are orthogonal to ξ_d , they must have negligible overlaps with the initial perturbation.

We have found that $\xi_d(r) \approx r^{m-1}\zeta'_0(r)$ for most vortices that have discrete modes. It follows that discrete modes (when they exist) generally dominate the excitation that is created by a $\delta(t)$ external impulse. Of course, if $\zeta'_0(r_c)$ is slightly negative, the impulse excites a weakly damped quasimode instead.

C. The response of a Gaussian vortex

In this section we examine the response of a Gaussian vortex to a $\delta(t)$ external impulse. As for top-hat vortices, the quadrupole moment of the perturbed Gaussian decays expo-

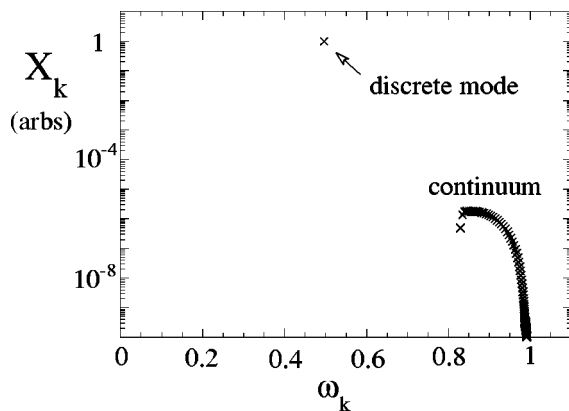


FIG. 7. The $m=2$ excitability spectrum for Top-Hat 1.

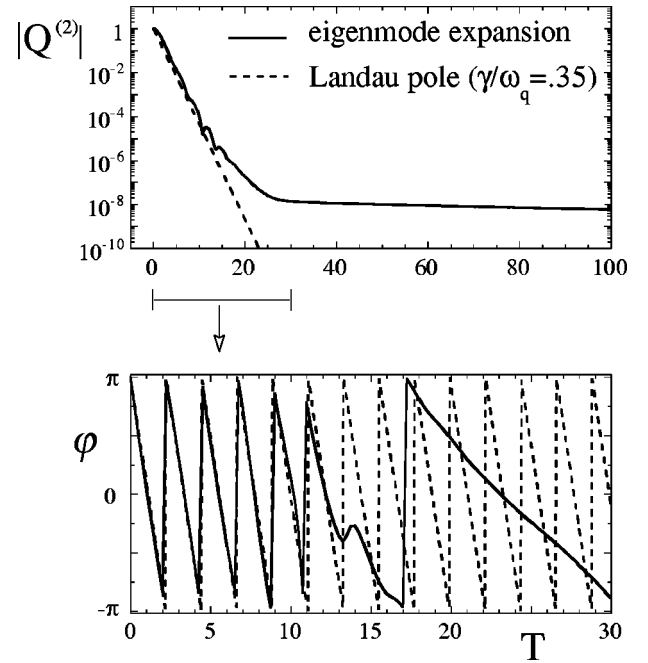


FIG. 8. Evolution of the quadrupole moment, $Q^{(2)}(t) \equiv |Q^{(2)}(t)|e^{i\varphi(t)}$, of a Gaussian vortex [Eq. (34)] after an external impulse. The solid lines give the complete linear evolution. The dashed lines give pure ‘‘Landau damping’’; that is $Q^{(2)} = e^{-\gamma t}e^{-i\omega_q t}$, where ω_q and γ are the real and imaginary parts of a Landau pole. $|Q^{(2)}(t)|$ is in units of $|Q^{(2)}(0)|$; $T = t\Omega_0(0)/2\pi$.

entially, and the decay rate is given by a Landau pole. However, the vorticity perturbation does not resemble a quasimode; rather, it becomes dominated by spiral filaments in a few vortex rotation periods.

The specific Gaussian vortex that we will study is given by

$$\zeta_0(r) = \exp[-(5r/R_w)^2], \quad (34)$$

for $r \leq R_v = 0.975R_w$. For $r \geq R_v$, ζ_0 is constant. This constant value of ζ_0 can be made zero by working in a rotating frame; in this sense, $\zeta_0(r)$ still fits our definition of a monotonic profile [Eq. (13)]. The Gaussian vortex that is defined by Eq. (34) does not have a discrete mode. Instead, all of its eigenmodes are continuum modes.

Figure 8 shows how the quadrupole moment $Q^{(2)}$ evolves after an $m=2$, $\delta(t)$ external impulse is applied to the Gaussian vortex. Before ten rotation periods, the phase of the quadrupole moment changes at a constant rate, and the amplitude $|Q^{(2)}|$ decays exponentially; that is, $Q^{(2)} \approx e^{-\gamma t}e^{-i\omega_q t}$. At ten rotation periods, the decay slows down.

Figure 8 also shows that ω_q and γ are accurately given by a Landau pole of the Gaussian vortex. For a Gaussian vortex, Eqs. (21) and (31) are poor approximations of the real part (ω_q) and imaginary part (γ) of the Landau pole. A more precise value for the Landau pole was calculated numerically (see Appendix B), using the method of Spencer and Rasband.¹⁶ This numerical calculation gave $\omega_q = 0.226$ and $\gamma = 0.079$.

Although ‘‘Landau damping’’ seems to dominate the initial decay, the excitation does not fit our definition of a quasimode. The vorticity perturbation is poorly described as

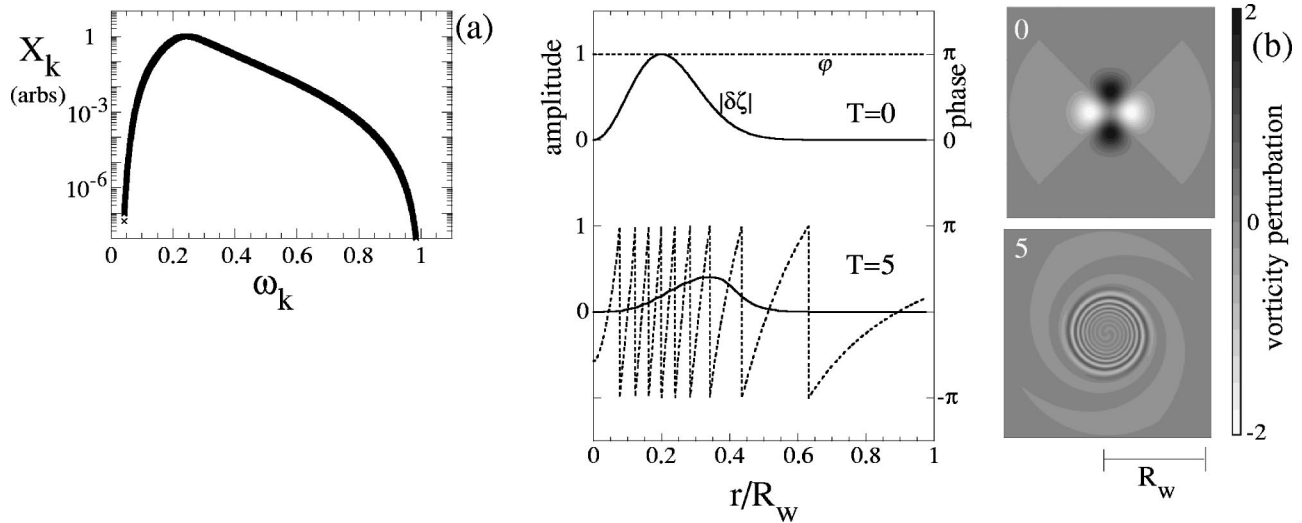


FIG. 9. Response of the Gaussian vortex [Eq. (34)] to an external impulse. (a) The excitability spectrum has a broad peak, in contrast to the sharply peaked frequency spectrum of a quasimode [e.g., Fig. 4(a)]. (b) The vorticity perturbation, $\Delta\zeta(r, \theta, t) = 2|\delta\zeta(r, t)|\cos[m\theta + \varphi(r, t)]$. The left graph in (b) shows the half-amplitude $|\delta\zeta|$ and phase φ of the perturbation as functions of the radius, at $T=0$ and at $T=5$ central rotation periods ($T \equiv t\Omega_0(0)/2\pi$). The right figures in (b) are contour plots of $\Delta\zeta$.

a single damped wave, which has the form $\xi(r)e^{-\gamma t}e^{i(m\theta - \omega_q t)} + c.c.$ Rather, as shown in Fig. 9(b), the vorticity perturbation is rapidly dominated by spiral filaments. This behavior is characteristic of a vortex that has a broad excitability spectrum [Fig. 9(a)], i.e., a vortex that has a Landau pole with a large imaginary part, $\gamma/\omega_q \sim 1$.

The mechanism for exponential damping can be removed on any vortex, including a Gaussian, by setting ζ'_0 equal to zero near the critical radius r_c of the Landau pole [$m\Omega_0(r_c) \equiv \omega_q$]. Figure 10(a) shows the Gaussian vortex of Eq. (34), with a plateau at r_c . The quadrupole moment of this modified Gaussian vortex does not decay exponentially after a brief external impulse. This is because the vortex supports an undamped discrete mode.

The discrete mode is shown directly below the equilibrium profile in Fig. 10(a). This mode has an eigenfrequency ω_d that is between the upper and lower limits of the continuum [Eq. (18)]; however, it is easily distinguished from a continuum mode. To begin with, the discrete mode does not have a singular spike at its critical radius. Furthermore, an external impulse will excite the discrete mode, but not the continuum modes with eigenfrequencies near ω_d [see Fig. 10(b)]. These continuum modes are not excited, because they would create a vorticity perturbation in the plateau region of ζ_0 , and an external impulse leaves this region unperturbed.

The discrete mode in Fig. 10 was created by *artificially* flattening the vorticity distribution at the critical radius r_c of the Landau pole; however, this process can also occur naturally during the nonlinear evolution of a vortex. For example, in the electron plasma experiments, vorticity filaments are wrapped into ‘‘cat’s eyes’’ in the vicinity of r_c [Fig. 1(a), far right]. If the vorticity distribution is θ averaged, these cat’s eyes correspond to an annulus of uniform vorticity. Since damping requires a finite vorticity gradient at r_c , the formation of cat’s eyes prevents further decay. The elliptical perturbation that remains in the vortex core after the initial de-

cay is approximately the undamped discrete mode of a vortex similar to the original, but flattened at r_c . It has been proposed that asymmetries in hurricanes may also develop into discrete modes during their nonlinear evolution, through a similar flattening of mean-flow vorticity.^{23,24}

As a final note, the excitability X_k in Fig. 10(b) was not obtained from Eq. (28). The inner-product in Eq. (28) is not defined when ζ'_0 vanishes anywhere inside the vortex. Instead, we used the formula $X_k = -\langle \xi_k^\dagger, r^{m-1} \zeta'_0 \rangle_s / \langle \xi_k^\dagger, \xi_k \rangle_s$,

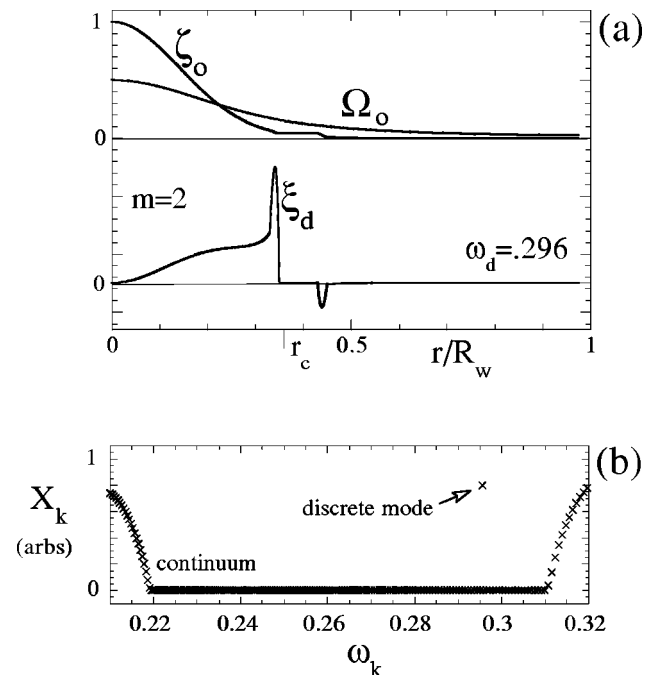


FIG. 10. Gaussian vortex with a flat interval. (a) Equilibrium profile and the $m=2$ discrete mode. r_c and ω_d denote the critical radius and the eigenfrequency of the discrete mode. (b) Excitability of the $m=2$ eigenmodes with frequencies near ω_d .

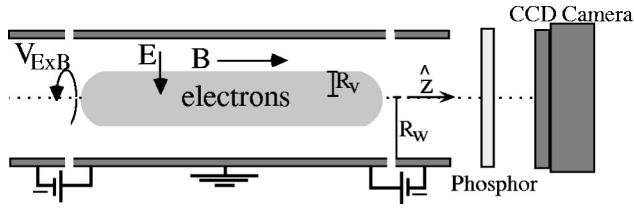


FIG. 11. Side view of a “Penning–Malmberg” apparatus that is used for studying 2-D Euler dynamics with a magnetized electron plasma.

and changed the normalization from Eq. (11) to $\langle \xi_k^\dagger, \xi_k \rangle_s = b$. Here, ξ_k^\dagger is the standard adjoint of the eigenfunction ξ_k , and $\langle f, h \rangle_s \equiv \int_0^{R_v} dr f^*(r) h(r)$. A derivation of this more general expression for excitability is straightforward, and is given in Ref. 35: it uses a “dual-space” formalism analogous to that found in Ref. 31.

IV. EXPERIMENTAL RESPONSE OF A MONOTONIC VORTEX TO AN EXTERNAL IMPULSE

We now directly compare linear response theory to the evolution of elliptical perturbations on two experimental vortices [Fig. 12]. We find that the initial exponential decay predicted by linear response theory is in good agreement with the experiments. Over longer times, the ellipticity exhibits nonlinear “trapping” oscillations, and then equilibrates at a finite amplitude.

A. Apparatus

Figure 11 is a schematic diagram of the experimental setup.^{6,7,38} A long column of electrons is confined in a hollow cylindrical conductor. Large dc voltages are applied on rings at both ends of the cylinder to keep the electrons from escaping in the axial (\hat{z}) direction. In addition, a uniform (1 T) magnetic field \mathbf{B} is applied parallel to the trap axis. This magnetic field counters the outward radial force of the electric field (\mathbf{E}) that is produced by the electron column, and thereby prevents the electrons from escaping to the wall.

The time period over which the electrons bounce from one end of the trap to the other (along the z axis) is much less than the characteristic time scale for the flow of electrons in the r – θ plane (i.e., a vortex rotation period). As a result, the

“instantaneous” r – θ velocity of an electron can be approximated by its average over a bounce period. The 2-D fluid equations obtained from this bounce-averaging scheme are known as the 2-D drift-Poisson equations:¹⁴

$$\frac{\partial n}{\partial t} + \mathbf{v} \cdot \nabla n = 0, \quad \mathbf{v} = \hat{z} \times c \nabla \phi / B, \quad \nabla^2 \phi = 4 \pi e n. \quad (35)$$

Above, $\mathbf{v}(r, \theta, t)$ is the $\mathbf{E} \times \mathbf{B}$ drift velocity field, $n(r, \theta, t)$ is the z -averaged electron density, and $\phi(r, \theta, t)$ is the electrostatic potential. The boundary condition is $\phi = 0$ at R_w , since the wall of the trap is grounded.

The equations for the vorticity of the r – θ flow can be obtained directly from Eq. (35). They are the 2-D Euler equations [Eq. (1)]. The stream function relates to the electrostatic potential by the equation $\psi \equiv c \phi / B$, and the vorticity relates to the electron density by the equation $\zeta = 4 \pi e c n / B$. The vacuum between the electron column and the conducting wall corresponds to a region of zero vorticity. The boundary condition $\phi = 0$ at the conducting wall corresponds to free slip at the wall of a circular container.

Because ζ is proportional to n , vorticity measurements are equivalent to density measurements. Thus, vorticity is measured by dumping the electrons onto a phosphor screen, and recording the density (vorticity) image with a charge-coupled device camera. Although this imaging is destructive, the initial conditions are reproducible, so that the time evolution of flows (e.g., Fig. 1) can be studied.

B. Evolution of elliptical perturbations

We now consider the evolution of elliptical perturbations on the two experimental vortices that are shown in Fig. 12. At $t = 0$, these vortices are perturbed by an external impulse. The impulse is created by briefly applying voltages to isolated 60° sections of the conducting wall.^{6,7} The voltages are phased spatially so as to mainly produce an $m = 2$ electrostatic potential (stream function). This potential deforms the initially circular vortex into an ellipse.

Figure 13 shows how the quadrupole moments of the two experimental vortices evolve after the impulse. In both experiments, the quadrupole moment $Q^{(2)}(t)$ exhibits an early stage of decay that is approximately exponential ($e^{-\gamma t}$). Furthermore, in both cases, the phase φ of the quad-

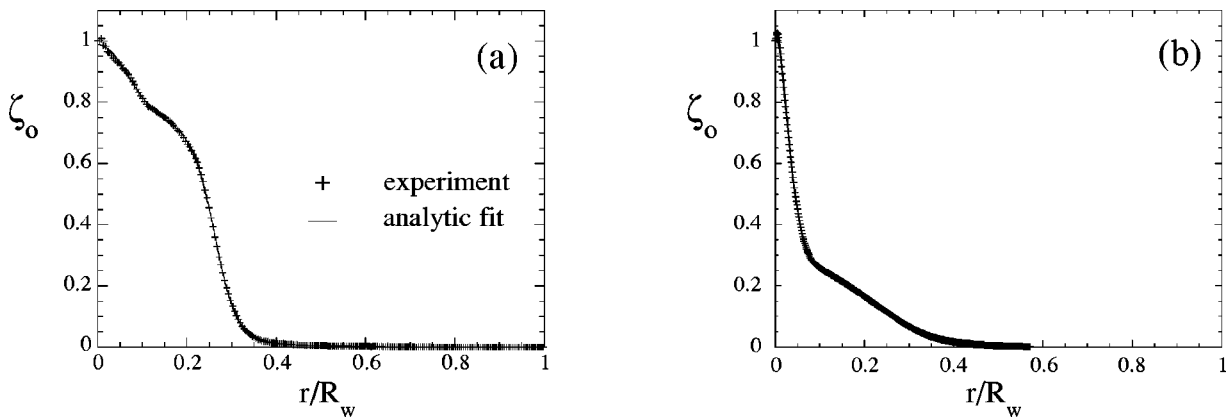


FIG. 12. Equilibrium vorticity profiles for two experimental vortices. The profile in (b) corresponds to the vortex in Fig. 1.

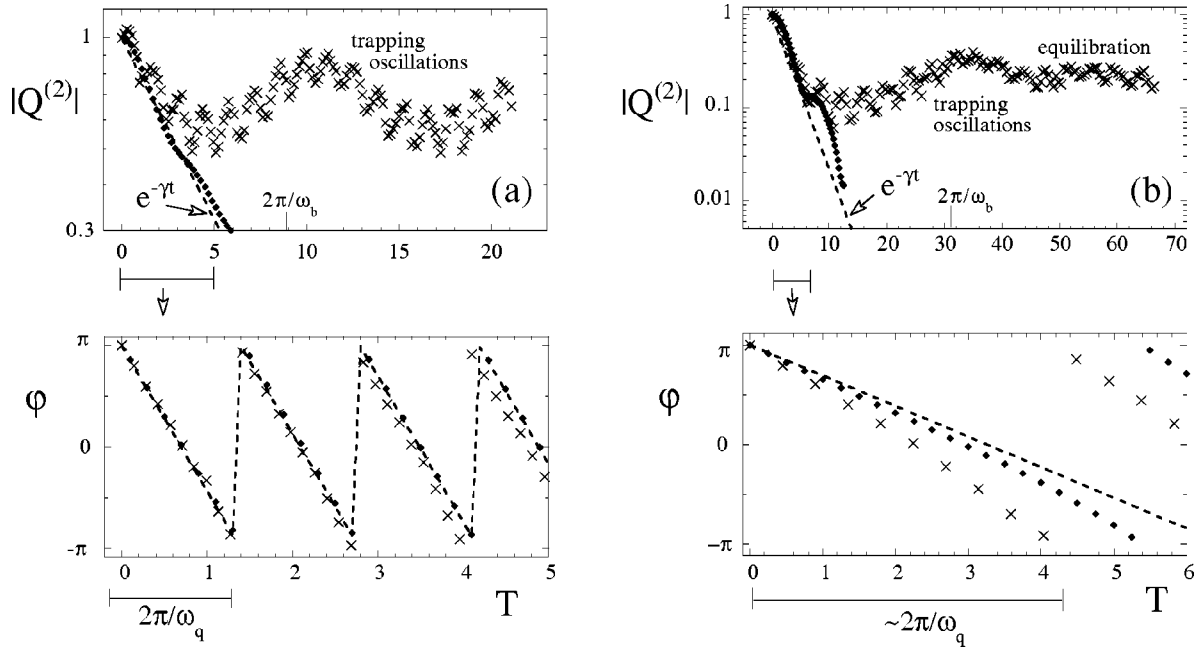


FIG. 13. Evolution of the quadrupole moment, $Q^{(2)}(t) \equiv |Q^{(2)}(t)|e^{i\phi(t)}$, in two typical experiments. The X's are experimental data, whereas the diamonds and dashed lines are theoretical predictions. The diamonds give the complete linear response of the vortex to an external impulse. The dashed lines show the contributions to $Q^{(2)}$ from the Landau poles, which dominate the early response in both cases. The equilibrium profiles for experiments (a) and (b) are shown in Figs. 12(a) and 12(b), respectively. $|Q^{(2)}(t)|$ is in units of $|Q^{(2)}(0)|$; $T \equiv t\Omega_0(0)/2\pi$.

rupole moment changes at a constant rate ω_q , i.e., the elliptical perturbation rotates with a constant angular velocity.

Figure 13 also compares the experimental data to linear response theory. Here, linear response theory assumes that the elliptical perturbation is created by a $\delta(t)$ impulse, and therefore that the initial vorticity perturbation is given by Eq. (30). In experiment (a) [Fig. 13(a)], there is good agreement between the early evolution of $Q^{(2)}$ and linear response theory. In experiment (b) [Fig. 13(b)], there is a noticeable ($\sim 20\%$) discrepancy between the experimental value of ω_q and linear theory. This frequency difference probably indicates that the initial experimental excitation is slightly nonlinear.

In Sec. III, we showed that the initial linear evolution of the quadrupole moment is generally dominated by a Landau pole contribution. This contribution varies with time exactly like $e^{-\gamma t}e^{-i\omega_q t}$, where ω_q and γ are the real and imaginary parts of the Landau pole. To calculate a Landau pole requires analytic continuations of both $\zeta_0(r)$ and $\Omega_0(r)$ in the complex r plane (see Appendix B, and Refs. 14–16). To obtain these continuations for an experimental vortex, we approximate the measured vorticity profile $\zeta_0(r)$ with a combination of analytic functions, such as Gaussians, hyperbolic tangents, and polynomials. The analytic continuation of $\Omega_0(r)$ is then obtained from its integral solution, $\Omega_0(r) = r^{-2} \int_0^r dr' r' \zeta_0(r')$, where r is complex. The solid lines in Fig. 12 show our analytic approximations of $\zeta_0(r)$ [evaluated along the real r axis] for both experiments. Using these approximations, we calculated the Landau poles numerically, as described in Appendix B. For experiment (a), we obtained a Landau pole with $\omega_q = 0.36$ and $\gamma = 0.018$ in units of $\zeta_0(0)$. For experiment (b), we obtained a Landau pole with $\omega_q = 0.077$ and $\gamma = 0.030$.

The dashed lines in Fig. 13 are the Landau pole contributions to $Q^{(2)}(t)$. It is evident from Fig. 13 that the Landau pole contribution accurately describes the initial evolution of $Q^{(2)}$ for experiment (a). For experiment (b), the Landau pole contribution gives an accurate value for γ , but gives a value for ω_q that is less than the experimental value, as did the complete linear response.

We now discuss the behavior of the vorticity perturbation. The vorticity perturbation in experiment (b) is heavily damped in the core, and is rapidly dominated by filaments. On the other hand, the vorticity perturbation in experiment (a) behaves like a single damped wave (quasimode) for several cycles. Specifically, the $m=2$ component of vorticity is well described by a fit^{7,38} of the form, $\delta\zeta(r,t) \approx \hat{\xi}(r)e^{-\hat{\gamma}t}e^{-i\hat{\omega}_q t}$, for $T \lesssim 5$. From the fit, we obtain $\hat{\omega}_q = 0.37 \pm 0.01$ and $\hat{\gamma} = 0.013 \pm 0.003$. Figure 14(a) shows the radial part $\hat{\xi}(r)$ of the quasimode that was obtained from the fit: it is roughly proportional to $r^{m-1}\zeta_0'(r)$, like the quasimode of a top-hat vortex.

Of course, $\hat{\omega}_q$ and $\hat{\gamma}$ are consistent with the observed frequency and decay rate of the quadrupole moment $Q^{(2)}$. Accordingly, they are in reasonable agreement with the calculated Landau pole, which has $\omega_q = 0.36$ and $\gamma = 0.018$. We now show that the radial part $\hat{\xi}(r)$ of the measured quasimode is also in good agreement with linear theory.

Figure 14(b) shows the $m=2$ excitability spectrum of the vortex in experiment (a). The excitability X_k [Eq. (28)] is shown as a function of the critical radius $r_{c,k}$ [Eq. (19)] of each continuum mode. The excitability has a moderately sharp peak, indicating that a brief external impulse excites a quasimode.

The radial part of the theoretical quasimode is approxi-

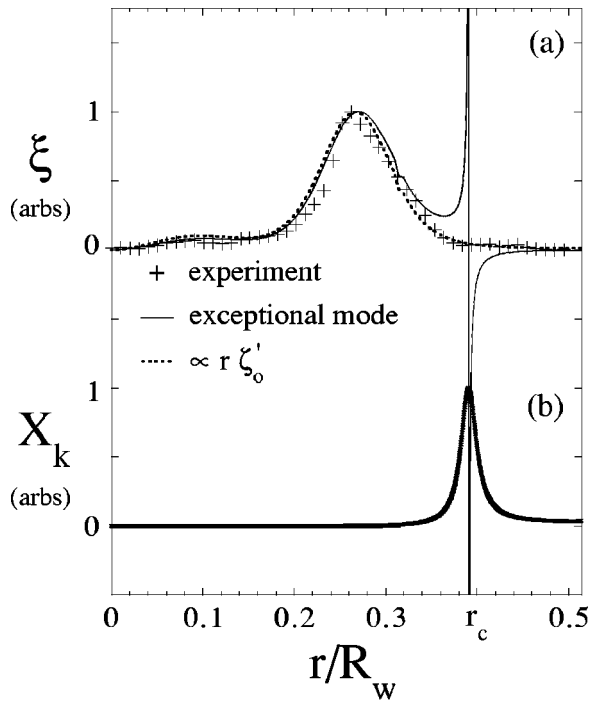


FIG. 14. The $m=2$ quasimode of an experimental vortex [Fig. 12(a)]. (a) The radial part $\xi(r)$ of the observed quasimode compared to theory. (b) Eigenmode excitability vs the critical radius $r_{c,k}$ of the eigenmode. The moderately sharp peak indicates that a brief external impulse excites a quasimode.

mately proportional to the radial eigenfunction of an “exceptional” continuum mode (for $r \lesssim r_{c,k}$), which has its critical radius in the peak region of excitability. In Fig. 14(a), the eigenfunction of an exceptional continuum mode is superposed (after being rescaled) on the radial part of the experimental quasimode. The two are in excellent agreement, for $r \lesssim r_{c,k}$.

After about five rotation periods, both experiments diverge from linear theory, and the amplitude of $Q^{(2)}$ slowly oscillates (Fig. 13). A critical eye will notice secondary oscillations, with frequency ω_q , in the experimental data. These small rapid oscillations should be ignored, since they are artifacts of inhomogeneities in the phosphor. We now compare the observed slow oscillation frequency of $|Q^{(2)}|$ to a theoretical estimate,¹⁴ which assumes that the perturbation is dominated by a single wave, i.e., a quasimode.

The amplitude of the quasimode changes with time to conserve the flow’s energy and angular momentum, as vorticity is phase mixed in the critical layer at r_c (see Appendix A). Early on, this phase-mixing causes the amplitude to decay at the exponential rate γ , given by linear theory. Over longer times, the vorticity perturbation becomes nonlinear in the critical layer, and the amplitude of the quasimode oscillates (“bounces”). As $t \rightarrow \infty$, the phase-mixing in the critical layer completes, and the amplitude of the quasimode equilibrates at a finite level.

The bounce frequency ω_b of the quasimode amplitude is estimated by considering the flow in the critical layer. In a frame that corotates with the quasimode, the streamlines in the critical layer are closed, forming “cat’s eyes” (Fig. 16,

Appendix A). One expects that ω_b is approximately the orbital frequency of a fluid particle that is “trapped” on a closed streamline. This frequency was estimated in Ref. 14:

$$\omega_b^2 = \frac{m^2}{r_c} |2\delta\psi(r_c)\Omega'_0(r_c)|. \quad (36)$$

Here, $|\delta\psi(r_c)|$ is the amplitude of the m th Fourier coefficient of the stream function perturbation evaluated at the critical radius r_c , and averaged over a bounce period.

For experiment (a), Eq. (36) yields $\omega_b = 0.056$ in units of $\zeta_0(0)$. For experiment (b), Eq. (36) yields $\omega_b = 0.016$. The bounce periods ($2\pi/\omega_b$) corresponding to these estimates are marked in Fig. 13. It is evident that the estimated bounce periods accurately give the oscillation periods of $|Q^{(2)}|$ in both experiments.

Further details of the nonlinear stages of the vortex evolution are beyond the scope of this paper, but are quantitatively addressed elsewhere.^{7,8,11,25} Here, we note that in principle the linear stage can be made arbitrarily long by decreasing the amplitude of the initial perturbation.

V. SUMMARY

In this paper we examined the inviscid damping of asymmetries on a 2-D circular vortex. We focused on the damping of elliptical perturbations that are created by an $m=2$ $\delta(t)$ external impulse. In linear theory, after the impulse, the phase of the quadrupole moment of the perturbed vortex changes at a constant rate ω_q , and the amplitude $|Q^{(2)}|$ of the quadrupole moment decays at an exponential rate γ . We showed that both ω_q and γ are given by a Landau pole of the equilibrium profile. After this initial period of exponential decay, linear theory predicts that there is a transition toward algebraic ($t^{-\alpha}$) decay.

We also showed that during the exponential decay of $|Q^{(2)}|$, the linear vorticity perturbation behaves in two distinct ways, depending on the order of magnitude of γ . For $\gamma/\omega_q \ll 1$, the vorticity perturbation is a quasimode, i.e., it behaves like a single exponentially damped wave in the vortex core ($r \lesssim r_c$). For $\gamma/\omega_q \sim 1$, the vorticity perturbation does not resemble a damped wave; rather, it becomes dominated by spiral filaments in a few vortex rotation periods.

The linear quasimode was analyzed as a packet of neutrally stable continuum modes. From this perspective, the quasimode decays through destructive interference as the continuum modes disperse. The exponential decay rate γ is proportional to $\zeta'_0(r_c)$, the vorticity gradient at the critical radius. Physically, the quasimode is damped by a resonant interaction with corotating fluid (see Appendix A). This resonant wave–fluid interaction is analogous to the well-known resonant wave–particle interaction in plasma physics,^{14,30,39} which can cause the exponential damping of Langmuir oscillations (for example).

The initial exponential decay predicted by linear theory was shown to agree with electron plasma experiments. However, the algebraic ($t^{-\alpha}$) decay predicted for late times^{17,28,29} was not observed experimentally. Instead, the amplitude of the quadrupole moment was found to equilibrate at a finite fraction of its initial value (Figs. 1 and 13). As discussed at

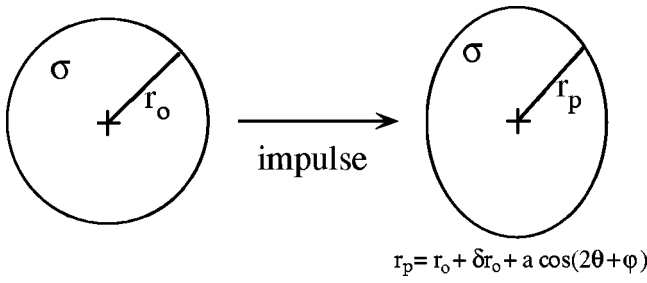


FIG. 15. Elliptical deformation of a uniform circular vortex patch.

the ends of Secs. III and IV, this equilibration is due to the wrapping of vorticity filaments at the critical radius r_c . Such wrapping causes the θ -averaged radial vorticity gradient to vanish at r_c , and thereby removes the mechanism for resonant damping (see Appendix A).

Under the right conditions, algebraic decay might occur in the experiments with magnetized electron plasmas. For example, we expect to observe algebraic decay at late times if the initial perturbation is sufficiently weak. Then, linear theory would apply for longer times, allowing a transition to algebraic decay, as in Fig. 5. Another possibility is to create an asymmetry by means other than an external impulse. For example, one could add onto the vortex a low-amplitude cloud of vorticity (electron cloud). If this cloud does not overlap strongly with a quasimode, the multipole moment(s) of the vortex can relax to time-asymptotic algebraic decay in less than one rotation period.

ACKNOWLEDGMENTS

This work was funded by the National Science Foundation (NSF-9876999) and the Office of Naval Research (N00014-96-1-0239).

APPENDIX A: DAMPING OF A QUASIMODE BY A RESONANT WAVE-FLUID INTERACTION

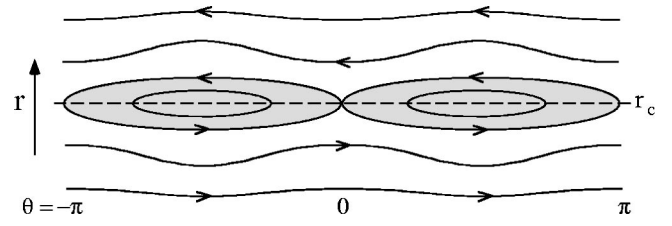
In this appendix, we explain how exponential damping results from a resonant wave-fluid interaction.^{14,30} We make explicit use of conservation of canonical angular momentum, $P_\theta \equiv \int d^2r r^2 \zeta$. Note that P_θ is a convenient simplification of the actual angular momentum per unit length \mathcal{L} , which is given by the equation $\mathcal{L} \equiv \hat{z} \cdot \int d^2r r \mathbf{r} \times \rho \mathbf{v} = \frac{1}{2} \rho (\Gamma R_w^2 - P_\theta)$. Here, ρ is the uniform mass density of the fluid, and Γ is the total circulation of the flow.

1. Angular momentum of the mode

For simplicity, we consider a uniform circular vortex patch of radius r_0 and vorticity $\sigma > 0$. Suppose that a ripple of azimuthal wave number m is created on the edge of the vortex patch, in such a way that the area of the (incompressible) vortex patch is conserved. Figure 15 illustrates this perturbation for the case of $m=2$. Here, the ripple corresponds to an elliptical deformation.

Let $r_p(\theta, t)$ describe the radius of the perturbed vortex patch. With the ripple,

$$r_p(\theta, t) = r_0 + \delta r_0(t) + a(t) \cos[m\theta + \varphi(t)]. \quad (\text{A1})$$


 FIG. 16. Kelvin's cat's eyes at the critical radius r_c .

Here $a(t)$ and $\varphi(t)$ are the amplitude and phase of the asymmetric part of the ripple. The symmetric part $\delta r_0(t)$ is required to conserve the area of the vortex patch. To lowest order, δr_0 is related to a by

$$\delta r_0 = -\frac{a^2}{4r_0}. \quad (\text{A2})$$

Note that Eq. (A1) neglects the growth of other asymmetries with wave numbers $m' \neq m$. This "single-wave model" is good, provided that a is small.

When the vortex patch is isolated, the ripple behaves like an undamped mode.³² Specifically, $a(t)$ is constant and $\varphi(t) = -\omega t$. Here, ω is approximately (σ times) the Kelvin frequency that is defined in Eq. (21).

The angular momentum $P_{\theta, M}$ of the mode is defined as the difference in P_θ between the vortex patch with and without the mode; that is,

$$P_{\theta, M} \equiv \int_0^{2\pi} d\theta \int_0^{r_p} dr r^3 \sigma - \int_0^{2\pi} d\theta \int_0^{r_0} dr r^3 \sigma. \quad (\text{A3})$$

Using Eq. (A1) for r_p , Eq. (A2) for δr_0 , and carrying out the integrals in Eq. (A3), we obtain the following expression (to lowest order in a) for the angular momentum of the mode:

$$P_{\theta, M} = \pi \sigma r_0^2 a^2. \quad (\text{A4})$$

2. Exponential damping of the mode

Now suppose that there is a low level ($\ll \sigma$) of vorticity outside the vortex patch, extending to the wall radius R_w . If this low level of vorticity decreases monotonically with r , it will cause the mode to decay.

To see this, we examine the flow at the critical radius r_c ($> r_0$), where the fluid rotation is resonant with the mode [$m\Omega_0(r_c) \equiv \omega$]. In a frame that rotates with the mode, the streamlines near r_c form cat's eyes.⁴⁰ These cat's eyes (gray) are illustrated in Fig. 16, for the case of $m=2$.

In time, the vorticity in the cat's eyes is mixed (phase mixed). Since $\zeta'_0(r_c) < 0$, this mixing increases the mean-square-radius of the flow (i.e., P_θ). The only way for the system to conserve total P_θ is for the mode amplitude a to decay.

The rate of change of the mode angular momentum is equal and opposite to the rate of change of P_θ in the skirt of low-level vorticity that is outside the vortex patch. Let $P_{\theta, s}$ denote the angular momentum in the skirt. The time derivative of $P_{\theta, s}$ can be expressed as the following integral:

$$\frac{d}{dt}P_{\theta,s} = 2\pi \int_0^{R_w} dr r^3 \frac{\partial}{\partial t} \delta\zeta_s^{(0)}. \quad (\text{A5})$$

Here, $\delta\zeta_s^{(0)}(r,t)$ is the axisymmetric ($m=0$) component of the vorticity perturbation in the skirt. From the Euler equation for the evolution of vorticity, we obtain (to lowest order)

$$\frac{\partial}{\partial t} \delta\zeta_s^{(0)} = -\frac{2}{r} \text{Im} \left[m \frac{\partial}{\partial r} (\delta\psi^{(m)} \delta\zeta_s^{(m)*}) \right], \quad (\text{A6})$$

where m is the azimuthal wave number of the mode, and Im denotes the imaginary part of the function in square brackets. As in the main text, $\delta\psi^{(m)}(r,t)$ is the m th Fourier coefficient of the stream function perturbation; similarly, $\delta\zeta_s^{(m)}(r,t)$ is the m th Fourier coefficient of the vorticity perturbation in the skirt. Substituting Eq. (A6) into Eq. (A5), and integrating by parts, we obtain

$$\frac{d}{dt}P_{\theta,s} = 8\pi m \int_0^{R_w} dr r \text{Im} [\delta\psi^{(m)} \delta\zeta_s^{(m)*}]. \quad (\text{A7})$$

We will assume that the stream function perturbation is dominated by the mode; that is,³²

$$\delta\psi^{(m)}(r,t) \approx \frac{a(t)}{2} \sigma r_0 G(r|r_0) e^{-i\omega t}. \quad (\text{A8})$$

Here, G is the Green's function that is defined by Eq. (6). In Eq. (A8), the phase $\varphi(t)$ of the mode is simply $-\omega t$. This neglects any phase perturbation due to the low-vorticity skirt.

To sufficient accuracy, the evolution of $\delta\zeta_s^{(m)}$ is obtained from the linearized Euler equation,

$$\frac{\partial}{\partial t} \delta\zeta_s^{(m)} + im\Omega_0(r) \delta\zeta_s^{(m)} - i \frac{m}{r} \zeta_0'(r) \delta\psi^{(m)} = 0. \quad (\text{A9})$$

Here, $\delta\psi^{(m)}$ is given by Eq. (A8), and is proportional to the mode amplitude a . The solution to Eq. (A9) is given by

$$\delta\zeta_s^{(m)}(r,t) = a \frac{m\sigma r_0}{2r} \frac{\zeta_0'(r) G(r|r_0)}{m\Omega_0(r) - \omega} [e^{-i\omega t} - e^{-im\Omega_0(r)t}], \quad (\text{A10})$$

provided that $\delta\zeta_s^{(m)}$ is initially zero, and that a is approximately constant over the integration period t .

Substituting Eqs. (A8) and (A10) into Eq. (A7) gives the following expression for the time derivative of the angular momentum in the skirt:

$$\begin{aligned} \frac{d}{dt}P_{\theta,s} &= -2\pi a^2 m^2 \sigma^2 r_0^2 \int_0^{R_w} dr G^2(r|r_0) \zeta_0'(r) \\ &\quad \times \frac{\sin[(m\Omega_0(r) - \omega)t]}{m\Omega_0(r) - \omega}. \end{aligned} \quad (\text{A11})$$

After a few cycles (i.e., $m\Omega_0 t \approx \omega t \gg 1$), the integrand in Eq. (A11) becomes sharply peaked at the critical radius r_c , defined by $m\Omega_0(r_c) \equiv \omega$, and the integral asymptotes to a constant value. This time-asymptotic value is given in the following:

$$\frac{d}{dt}P_{\theta,s} = -2\pi^2 a^2 m \sigma^2 r_0^2 G^2(r_c|r_0) \frac{\zeta_0'(r_c)}{|\Omega_0'(r_c)|}. \quad (\text{A12})$$

By conservation of angular momentum, the time derivative of the mode angular momentum must balance the time derivative of the angular momentum in the skirt; that is,

$$\frac{d}{dt}P_{\theta,M} = -\frac{d}{dt}P_{\theta,s}. \quad (\text{A13})$$

We will use Eq. (A12) for the time derivative of $P_{\theta,s}$, with a now a function of time. This approximation is good, provided that the mode amplitude a varies slowly compared to the rate at which $dP_{\theta,s}/dt$ equilibrates, under the condition of fixed a . That is, the decay rate γ of the mode must satisfy $\gamma/\omega \ll 1$.

Substituting Eqs. (A4) and (A12) into Eq. (A13), we obtain

$$\frac{d}{dt}a^2 = \frac{\pi}{2m} r_0 \zeta_0'(r_c) \left(\frac{r_0}{r_c} \right)^{2m-3} \left[1 - \left(\frac{r_c}{R_w} \right)^{2m} \right]^2 a^2. \quad (\text{A14})$$

Here, we have used $\Omega_0' = -\sigma r_0^2/r^3$ ($r > r_0$), and Eq. (6) for the Green's function G . The solution to Eq. (A14) is $a(t) = a(0)e^{-\gamma t}$, where the decay rate γ is given as follows:

$$\gamma = \frac{-\pi}{4m} r_0 \zeta_0'(r_c) \left(\frac{r_0}{r_c} \right)^{2m-3} \left[1 - \left(\frac{r_c}{R_w} \right)^{2m} \right]^2. \quad (\text{A15})$$

This decay rate is the imaginary part of the Landau pole [Eq. (31)] that was calculated by Briggs, Daugherty and Levy.¹⁴

Note that when $\zeta_0'(r_c) > 0$, mixing at r_c decreases P_θ in the skirt. In this case, the amplitude a of the mode must increase to conserve angular momentum. In other words, positive vorticity gradient at r_c leads to an instability. This instability is evident in Eq. (A15), which gives a positive growth rate (negative γ) when $\zeta_0'(r_c) > 0$.

APPENDIX B: LANDAU POLES

In this appendix, we review how to calculate numerically the Landau poles of a monotonic vortex. We present a brief summary (without derivations) of the main points in Refs. 14–16, and refer the reader to these articles for greater detail, and a more precise treatment.

Note that Refs. 14–16 discuss the evolution of the stream function perturbation and its derivatives. In this paper, we examine the evolution of the multipole moment $Q(t)$, which is defined by Eq. (12). The multipole moment is related to the stream function perturbation by the following:

$$Q(t) = (R_w)^{m+1} \frac{\partial \delta\psi}{\partial r}(R_w, t).$$

1. The Laplace transform of the multipole moment

The multipole moment $Q(t)$, of a perturbation that varies like $e^{im\theta}$ can be written formally as a contour integral in the complex ω plane:

$$Q(t) = -\frac{1}{2\pi} \int_{+\infty+i\alpha}^{-\infty+i\alpha} d\omega \tilde{Q}(\omega) e^{-i\omega t}, \quad (\text{B1})$$

where α is a positive real number. We will refer to the contour of integration in Eq. (B1) as the ‘‘inversion contour.’’ The function $\tilde{Q}(\omega)$ is the usual Laplace transform, defined by $\tilde{Q}(\omega) = \int_0^\infty dt Q(t) e^{i\omega t}$.

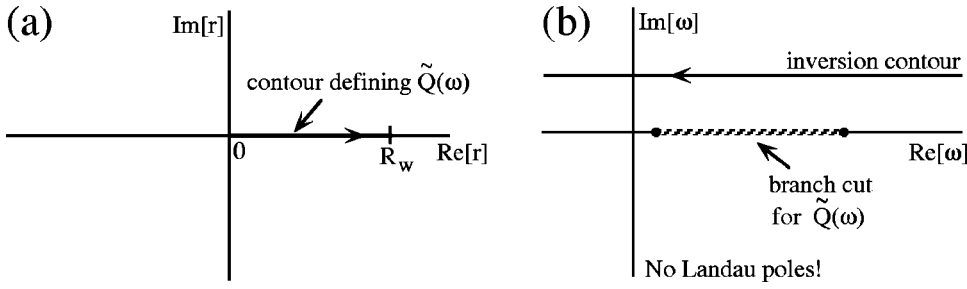


FIG. 17. When (a) the radial integration contour is along the real r axis, (b) there are no poles in $\tilde{Q}(\omega)$ that correspond to discrete zeros of $\Psi_1(R_w, \omega)$.

A solution for $\tilde{Q}(\omega)$, in terms of the initial vorticity perturbation $\delta\zeta(r, 0)$, can be extracted from the literature:^{14–16}

$$\begin{aligned}\tilde{Q}(\omega) &= \frac{i(R_w)^{m+1}}{\Psi_1(R_w, \omega)} \int_0^{R_w} dr \frac{r}{R_w} \frac{\Psi_1(r, \omega) \delta\zeta(r, 0)}{\omega - m\Omega_0(r)} \\ &\equiv \frac{\mathcal{N}(\omega)}{\Psi_1(R_w, \omega)}.\end{aligned}\quad (\text{B2})$$

Here, the function $\Psi_1(r, \omega)$ is a solution to

$$\left[\frac{1}{r} \frac{\partial}{\partial r} r \frac{\partial}{\partial r} - \frac{m^2}{r^2} + \frac{m}{r} \frac{\zeta'_0(r)}{\omega - m\Omega_0(r)} \right] \Psi_1(r, \omega) = 0, \quad (\text{B3})$$

which also satisfies $\Psi_1(0, \omega) = 0$. Equation (B3) is the same ordinary differential equation that must be satisfied by the stream function, $\Psi(r, \omega)e^{i(m\theta - \omega t)}$, of an eigenmode of the vortex. However, Ψ_1 need not vanish at $r = R_w$, as does the stream function of an eigenmode.

Suppose that the vortex extends to the wall (i.e., $R_v = R_w$), so that there are no discrete eigenmodes of the vortex.¹⁴ Then, there are no discrete values of ω , for which $\Psi_1(R_w, \omega) = 0$. The analytic properties of $\tilde{Q}(\omega)$ for this case are shown schematically in Fig. 17. There are no poles in $\tilde{Q}(\omega)$ that correspond to discrete zeros of $\Psi_1(R_w, \omega)$, but there is a branch cut along the real ω axis, in the interval $m\Omega_0(R_w) < \omega < m\Omega_0(0)$.^{14–16}

It is possible to deform the branch cut below the real ω axis by deforming the radial contour of integration in Eq. (B2) above the real r axis.^{14–16} The new branch cut, defined by $m\Omega_0(\text{Re}[r] + i\text{Im}[r]) = \omega$, is sketched in Fig. 18. If the branch cut in the complex ω plane bends sufficiently far below the real axis, a Landau pole ($\omega = \omega_q - i\gamma$) will appear in the analytic continuation of $\tilde{Q}(\omega)$, between the branch cut and the real ω axis.

The Landau pole corresponds to a discrete zero of $\Psi_1(R_w, \omega)$. This discrete zero is now possible, since $\Psi_1(r, \omega)$ is defined along the deformed radial contour [Fig.

18(a)], and not the real r axis. So, the Landau pole can be calculated by finding a discrete mode of Eq. (B3), along the deformed radial contour. The boundary conditions on this unphysical discrete mode are $\Psi_1(0, \omega) = \Psi_1(R_w, \omega) = 0$.

The inversion integral [Eq. (B1)] can be deformed around the Landau pole and the branch cut, as illustrated in Fig. 19. The contribution from the Landau pole gives a term in $Q(t)$ that is proportional to $e^{-\gamma t} e^{-i\omega_q t}$. As we have seen, this term dominates the early evolution of $Q(t)$, when the initial perturbation is caused by an external impulse.

Note that the locations of Landau poles in the complex ω plane are determined solely by the equilibrium profile $\zeta_0(r)$, and have no relation to the initial perturbation.

2. Numerical computation of a Landau pole

In Sec. III, we examined the response of a Gaussian vortex to an external $m=2$ impulse. We showed that the initial evolution of the quadrupole moment was dominated by the Landau pole. In this section, we discuss specifically how this pole was computed. A similar procedure was used to calculate the Landau poles of the experimental profiles in Sec. IV.

As mentioned previously, a Landau pole is a solution to the mode equation [Eq. (B3)] along a deformed contour in the complex r plane. The specific contour that we used to calculate the Landau pole of the Gaussian vortex [Eq. (34)] is the following parabola:

$$r(s) = R_w[s + i(s - s^2)], \quad (\text{B4})$$

where s is a real parameter, which satisfies $0 \leq s \leq 1$.

The mode equation [Eq. (B3)] can be rewritten as a differential equation in s ,

$$\left[\frac{\partial}{\partial s} \frac{r(s)}{r'(s)} \frac{\partial}{\partial s} - \frac{r'(s)m^2}{r(s)} + \frac{mr'(s)\zeta'_0[r(s)]}{\omega - m\Omega_0[r(s)]} \right] \Psi_1(s, \omega) = 0, \quad (\text{B5})$$

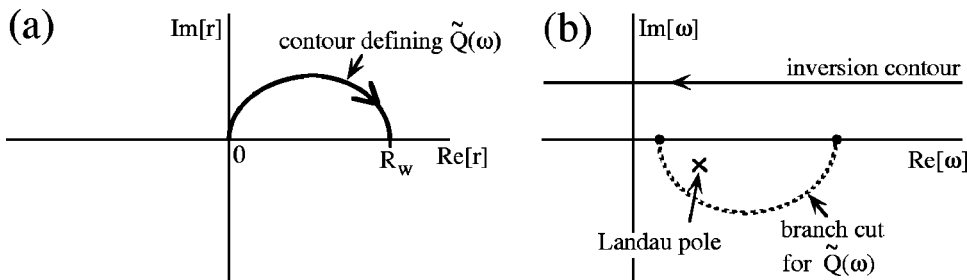


FIG. 18. When (a) the radial integration contour is deformed into the upper half-plane, (b) a Landau pole appears in $\tilde{Q}(\omega)$.

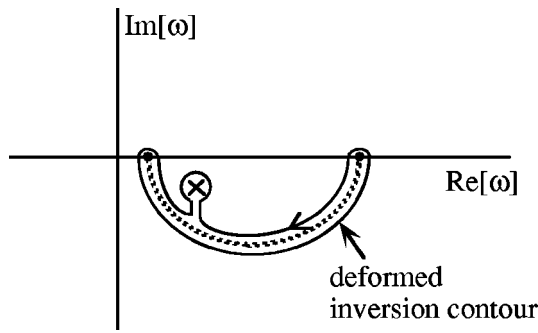


FIG. 19. The inversion contour can be deformed to wrap around the branch cut and the Landau pole. The contribution from the Landau pole gives a term in $Q(t)$ that decays exponentially.

where $\hat{\Psi}_1(s, \omega) \equiv \Psi_1(r(s), \omega)$, and $r'(s) = R_w[1 + i(1 - 2s)]$. The asymptotic form of $\Psi_1(r, \omega)$ is r^m , as $r \rightarrow 0$. This implies that $\hat{\Psi}_1(s, \omega)$ must satisfy the following initial conditions at $s \equiv \epsilon \ll 1$:

$$\begin{aligned} \text{(i)} \quad & \hat{\Psi}_1(\epsilon, \omega) = r^m(\epsilon), \\ \text{(ii)} \quad & \frac{\partial \hat{\Psi}_1}{\partial s}(\epsilon, \omega) = m r'(\epsilon) r^{m-1}(\epsilon). \end{aligned} \quad (\text{B6})$$

The value of ϵ is typically $\sim 10^{-3}$, and the accuracy of the solution improves as $\epsilon \rightarrow 0$.

The Landau pole is the complex value of ω that yields $\hat{\Psi}_1(1, \omega) = 0$. This value of ω is found using a standard shooting technique. For the Gaussian vortex in Eq. (34), we obtained the following value for the Landau pole: $\omega = 0.226 - 0.079i$.

- ¹D. G. Dritschel and B. Legras, "Modeling oceanic and atmospheric vortices," *Phys. Today* **46**(3), 44 (1993).
- ²J. Pedlosky, *Geophysical Fluid Dynamics* (Springer-Verlag, New York, 1987).
- ³A. P. Ingersoll, "Atmospheric dynamics of outer planets," *Science* **248**, 308 (1990).
- ⁴P. S. Marcus, "Numerical simulations of Jupiter's Great Red Spot," *Nature* **331**, 693 (1988).
- ⁵C. F. Driscoll, K. S. Fine, X.-P. Huang, T. B. Mitchell, and B. P. Cluggish, "Vortices and turbulent relaxation in magnetized electron columns," in *Transport, Chaos and Plasma Physics 2*, edited by S. Benkadda, F. Doveil, and Y. Elsken (World Scientific, Singapore, 1996).
- ⁶C. F. Driscoll and K. S. Fine, "Experiments in vortex dynamics in pure electron plasmas," *Phys. Fluids B* **2**, 1359 (1990).
- ⁷A. C. Cass, "Experiments on vortex symmetrization in magnetized electron columns," Ph.D. dissertation, University of California at San Diego, 1998.
- ⁸S. Pillai and R. W. Gould, "Damping and trapping in 2-D inviscid fluids," *Phys. Rev. Lett.* **73**, 2849 (1994).
- ⁹T. B. Mitchell and C. F. Driscoll, "Symmetrization of 2-D vortices by beat-wave damping," *Phys. Rev. Lett.* **73**, 2196 (1994).
- ¹⁰M. V. Melander, J. C. McWilliams, and N. J. Zabusky, "Axisymmetrization and vorticity-gradient intensification of an isolated two-dimensional vortex through filamentation," *J. Fluid Mech.* **178**, 137 (1987).
- ¹¹D. A. Bachman, "Nonlinear phenomena in a pure electron plasma studied with a 2-D fluid code," Ph.D. dissertation, California Institute of Technology, 1997.
- ¹²P. Koumoustakos, "Inviscid axisymmetrization of an elliptical vortex," *J. Comput. Phys.* **138**, 821 (1998).
- ¹³D. G. Dritschel, "On the persistence of non-axisymmetric vortices in inviscid two-dimensional flows," *J. Fluid Mech.* **371**, 141 (1998).

- ¹⁴R. J. Briggs, J. D. Daugherty, and R. H. Levy, "Role of Landau damping in crossed-field electron beams and inviscid shear flow," *Phys. Fluids* **13**, 421 (1970).
- ¹⁵N. R. Corngold, "Linear response of the two-dimensional pure electron plasma: Quasimodes for some model profiles," *Phys. Plasmas* **2**, 620 (1995).
- ¹⁶R. L. Spencer and S. N. Rasband, "Damped diocotron quasi-modes of nonneutral plasmas and inviscid fluids," *Phys. Plasmas* **4**, 53 (1997).
- ¹⁷A. P. Bassom and A. D. Gilbert, "The spiral wind-up of vorticity in an inviscid planar vortex," *J. Fluid Mech.* **371**, 109 (1998).
- ¹⁸A. J. Bernoff and J. F. Lingeitch, "Rapid relaxation of an axisymmetric vortex," *Phys. Fluids* **6**, 3717 (1994).
- ¹⁹J. F. Lingeitch and A. J. Bernoff, "Distortion and evolution of a localized vortex in an irrotational flow," *Phys. Fluids* **7**, 1015 (1995).
- ²⁰T. S. Lundgren, "Strained spiral vortex model for turbulent fine structure," *Phys. Fluids* **25**, 2193 (1982).
- ²¹M. T. Montgomery and R. J. Kallenbach, "A theory of vortex Rossby-waves and its application to spiral bands and intensity changes in hurricanes," *Q. J. R. Meteorol. Soc.* **123**, 435 (1996).
- ²²G. B. Smith II and M. T. Montgomery, "Vortex axisymmetrization: Dependence on azimuthal wave-number or asymmetric radial structure changes," *Q. J. R. Meteorol. Soc.* **121**, 1615 (1995).
- ²³M. T. Montgomery and J. Enagonio, "Tropical cyclogenesis via convectively forced vortex Rossby waves in a three-dimensional quasigeostrophic model," *J. Atmos. Sci.* **55**, 3176 (1997).
- ²⁴J. D. Moller and M. T. Montgomery, "Vortex Rossby waves and hurricane intensification in a barotropic model," *J. Atmos. Sci.* **56**, 1674 (1999).
- ²⁵N. J. Balmforth, S. G. Llewellyn Smith, and W. R. Young, "Disturbing vortices" (unpublished).
- ²⁶G. G. Sutyryn, "Azimuthal waves and symmetrization of an intense vortex," *Sov. Phys. Dokl.* **34**, 104 (1989).
- ²⁷M. T. Montgomery and C. Lu, "Free waves in barotropic vortices. Part I: Eigenmode structure," *J. Atmos. Sci.* **54**, 1868 (1997).
- ²⁸W. McF. Orr, "Stability and instability of steady motions of a perfect liquid," *Proc. Ir. Acad. Sect. A, Math Astron. Phys. Sci.* **27**, 9 (1907).
- ²⁹S. N. Brown and K. Stewartson, "On the algebraic decay of disturbances in a stratified linear shear flow," *J. Fluid Mech.* **100**, 811 (1980).
- ³⁰A. V. Timofeev, "Resonance effects in oscillations of nonuniform flows of continuous media," in *Reviews of Plasma Physics*, edited by B. B. Kadomtsev (Consultants Bureau, New York, 1992), Vol. 17, p. 193.
- ³¹C. Rivest and B. F. Farrell, "Upper-tropospheric synoptic-scale waves. Part II: Maintenance and excitation of quasi modes," *J. Atmos. Sci.* **49**, 2120 (1992).
- ³²Sir W. Thomson, "On the vibrations of a columnar vortex," *Philos. Mag.* **10**, 155 (1880); Sir H. Lamb, *Hydrodynamics*, 6th ed. (Dover, New York, 1945), p. 231.
- ³³K. M. Case, "Stability of inviscid plane Couette flow," *Phys. Fluids* **3**, 143 (1960).
- ³⁴P. G. Drazin and W. H. Reid, *Hydrodynamic Stability* (Cambridge University Press, Cambridge, 1981), pp. 150–151.
- ³⁵D. A. Schecter, "On the dynamics of inviscid relaxation in 2-D fluids and nonneutral plasmas," Ph.D. dissertation, University of California at San Diego, 1999.
- ³⁶Here, we solve the matrix eigenvalue problem with the double-precision LAPACK routine, DGEEV; E. Anderson *et al.*, *LAPACK Users' Guide*, 3rd ed. (Society for Industrial and Applied Mathematics, Philadelphia, PA, 1999).
- ³⁷The stability of monotonic vortices follows from the cylindrical analog to Rayleigh's inflection point theorem, which can be found in Ref. 14. The same theorem permits the instability of nonmonotonic vortices.
- ³⁸C. F. Driscoll, "Observation of an unstable $l=1$ diocotron mode on a hollow electron column," *Phys. Rev. Lett.* **64**, 645 (1990).
- ³⁹L. Landau, "On the vibration of the electronic plasma," *J. Phys. U.S.S.R.* **10**, 25 (1946); N. G. Van Kampen, "On the theory of stationary waves in plasmas," *Physica (Amsterdam)* **21**, 949 (1955); K. M. Case, "Plasma oscillations," *Ann. Phys. (N.Y.)* **7**, 349 (1959); T. M. O'Neil, "Collisionless damping of nonlinear plasma oscillations," *Phys. Fluids* **8**, 2255 (1965); F. F. Chen, *Introduction to Plasma Physics and Controlled Fusion* (Plenum, New York, 1990), Vol. 1.
- ⁴⁰Sir W. Thomson, "On a disturbing infinity in Lord Rayleigh's solution for waves in a plane vortex stratum," *Nature (London)* **23**, 45 (1880).